

Gravitating vortons as ring solitons in general relativity

Jutta Kunz, Eugen Radu and Bintoro Subagyo

Institut für Physik, Universität Oldenburg, Postfach 2503 D-26111 Oldenburg, Germany

July 31, 2021

Abstract

Vortons can be viewed as (flat space-) field theory analogs of black rings in general relativity. They are made from loops of vortices, being sustained against collapse by the centrifugal force. In this work we discuss such configurations in the global version of Witten's $U(1) \times U(1)$ theory. We first consider solutions in a flat spacetime background and show their nonuniqueness. The inclusion of gravity leads to new features. In particular, an ergoregion can occur. Also, similar to boson stars, we show that the vortons exist only in a limited frequency range. The coupling to gravity gives rise to a spiral-like frequency dependence of the mass and charge. New solutions of the model describing 'semitopological vortons' and 'di-vortons' are also discussed.

1 Introduction

Vortons are certainly among the most interesting particle-like solutions in field theory. Within a rather informal definition, they are ring-like solitons in some nonlinear field theory which is supposed to possess also string-like vortex solutions. Then the heuristic construction of a vorton involves taking a piece of finite length of such a vortex, bending it and gluing its ends to form a loop. The resulting configuration –the vorton, necessarily carries a nonzero angular momentum, such that the tension of the loop is compensated by the centrifugal force. This stationary ring does not radiate classically, and at large distances looks like a point particle with quantized charge and angular momentum.

Vortons were initially proposed 25 years ago [1, 2, 3] in the context of the local $U(1) \times U(1)$ theory of superconducting cosmic strings of Witten [4]. This model possesses vortex solutions with a non-dissipative current flowing along the string due to a complex scalar field which vanishes asymptotically. Vortons are closed loops of such superconducting strings, carrying both current and charge. However, vortons may exist in a variety of other theories as well, ranging from cosmology [5] to QCD [6] and condensed matter systems [7]. One can speculate that vortons may perhaps even exist in the Standard Model of Particle Physics.

The study of vortons has been a fruitful avenue of research since its inception. Some of the ideas which appeared in this context have found interesting applications in other domains of physics. For example, vortons share the same heuristic construction with black rings in $d \geq 5$ general relativity [8, 9], with vortices playing the role of black strings there. Moreover, a general formalism proposed by Carter in [10] to describe the properties of large radius vortons has found recently beautiful applications and generalizations in the physics of blackfolds in higher dimensional Einstein gravity [11].

At the same time, different from black rings in general relativity¹, there are no closed form vorton solutions. Moreover, even the numerical study of such configurations is difficult, due to the existence of multiple scales in the problem and the complicated behaviour of the matter functions.

In fact, to our knowledge there is no explicit construction in the literature of vorton solutions in a model containing gauge fields. However, by now, there are a number of independent studies of vortons in the global version of Witten's $U(1) \times U(1)$ model, which contains only two complex scalars. The numerical study of

¹Note, however, that the black rings are known in closed form for $d = 5$ spacetime dimensions only [8]. The $d > 5$ black rings were studied based on analytical solutions valid in the large radius limit [9] or on numerical nonperturbative solutions [12].

such solutions has started with the work of Lemperier and Shellard in Ref. [13]. There, the full hyperbolic evolution problem for the fields, with the initial data corresponding to a vortex loop has been considered. The results in [13] suggested the existence of vortons which are stable against perturbations. However, not so many details on the properties of such configurations were given there. In addition, Lemperier and Shellard did not consider precisely the rigid version of Witten’s model, but, in order to improve the numerics, added an extra Q-ball type interaction term.

The existence of stationary, axially symmetric vortons in Witten’s model has been reported in Ref. [14]. There, the solutions have been constructed by solving a set of elliptic partial differential equations with suitable boundary conditions². The configurations in [14] possess a nonzero value of the angular momentum and have ring profiles, describing thick vortons. Also, the results there point towards the existence of some analogies between vortons and spinning Q-balls in a simpler model with a single scalar field with a non-renormalizable potential [16, 17].

Large radius vortons have been reported in [18] for a different choice of the parameters of Witten’s model and a different numerical approach than the one employed in [14]. Ref. [18] has investigated also the numerical stability of such configurations with respect to non-axially symmetric perturbations. The results there show that (at least) thin vortons possess a pinching instability.

The main purpose of this work is to enlarge our understanding of vortons by including the effects of gravity, at a nonperturbative level. This is a legitimate task since the geometry in the vorton’s core may exhibit large deviations from the flat spacetime limit. Also, as shown by a number of other models [19, 20, 21], the inclusion of gravity usually leads to a variety of new effects. Indeed, as we shall see, this is also the case for vortons. For example, they may possess an ergoregion, with the associated instability. Also, gravitating vortons exhibit a rather different type of frequency dependence.

However, as a first step towards this task, we shall start with a study of vortons in a flat spacetime background. The solutions are easier to study in this limit, while some of their basic properties remain unaffected by the inclusion of gravity. Based on the heuristic construction of vortons as pieces of vortices, we propose a classification of the resulting objects in terms of an integer k related to the winding along a torus generator. Then it follows that vortons can be viewed as the second member ($k = 1$) of a general family of solutions. An unexpected result reported here is the nonuniqueness of vortons, that is the existence of different solutions for the same input parameters. Apart from solutions already known in the literature, new types of configurations, in particular those describing di-vortons, are also shown here.

This paper is organized as follows. In Section 2 we recall Witten’s gravitating global model, and give a precise formulation of the problem we propose to solve. We continue in Section 3 with a discussion of the properties of vortons in a flat spacetime background. The effects of gravity on the properties of vortons are discussed in Section 4. Two kinds of solutions are described there, corresponding to ‘semitopological’ vortons and ‘true’ vortons. Section 5 gives our conclusions together with a discussion of possible generalizations and open problems. In the Appendices we present the system of differential equations solved in this work (A), the components of the energy-momentum tensor (B), and the spherically symmetric limit of our solutions (C).

2 The model

2.1 The action and field equations

Witten’s ungauged model of superconducting cosmic strings [4] contains two complex scalar fields ϕ and σ , with the following Lagrangian density³

$$L_s = \partial_\mu \phi^* \partial^\mu \phi + \partial_\mu \sigma^* \partial^\mu \sigma + U(|\phi|, |\sigma|), \quad (2.1)$$

²An independent construction of these solutions has been reported in [15], based on a very different treatment of the numerical problem.

³Note that, as opposed to previous studies [13, 14, 18], we are using in this work a mostly plus signature for the spacetime metric.

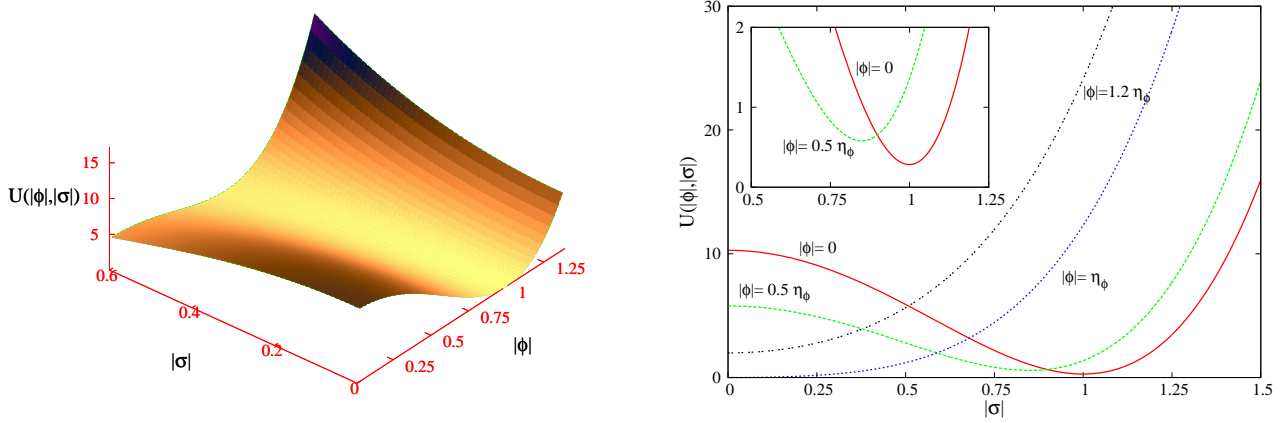


Figure 1. The potential $U(|\phi|, |\sigma|)$ of the model is shown for a set of parameters with $\eta_\phi = \eta_\sigma = 1$, $\lambda_\phi = 41$, $\lambda_\sigma = 40$, $\gamma = 22$. One can notice the existence of a single global minimum at $|\phi| = \eta_\phi$, $|\sigma| = 0$.

where $U(|\phi|, |\sigma|)$ is the scalar fields potential

$$U(|\phi|, |\sigma|) = \frac{1}{4}\lambda_\phi(|\phi|^2 - \eta_\phi^2)^2 + \frac{1}{4}\lambda_\sigma|\sigma|^2(|\sigma|^2 - 2\eta_\sigma^2) + \gamma|\phi|^2|\sigma|^2. \quad (2.2)$$

In the above potential, $\lambda_\phi, \lambda_\sigma, \eta_\phi, \eta_\sigma$ and γ are positive constants which are not specified apriori. A minimal value of the potential is achieved for $|\phi| = \eta_\phi$, $|\sigma| = 0$, in which case $U(|\phi|, |\sigma|) = 0$ (see Figure 1). This minimum is globally unique and stable if

$$4\gamma^2 > \lambda_\sigma\lambda_\phi \quad \text{and} \quad \gamma\eta_\phi^2 > \frac{1}{2}\lambda_\sigma\eta_\sigma^2. \quad (2.3)$$

Then the perturbative spectrum of the field excitations around the vacuum state $|\phi| = \eta_\phi$, $|\sigma| = 0$ consists of two massless Goldstone particles, corresponding to excitations of the phases of the fields, and of two Higgs bosons with the masses

$$M_\phi = \sqrt{\lambda_\phi}\eta_\phi, \quad M_\sigma = \sqrt{\gamma\eta_\phi^2 - \frac{1}{2}\lambda_\sigma\eta_\sigma^2}. \quad (2.4)$$

When coupling to gravity, the dynamics of the solutions is governed by the following action

$$S = \int d^4x \sqrt{-g} \left(\frac{R}{16\pi G} - L_s \right), \quad (2.5)$$

where g is determinant of the spacetime metric $g_{\mu\nu}$, G is Newton's constant and R is the curvature scalar. As usual in general relativity, variation of the action with respect to the metric leads to the Einstein equations

$$E_{\mu\nu} = R_{\mu\nu} - \frac{1}{2}g_{\mu\nu}R - 8\pi G T_{\mu\nu} = 0, \quad (2.6)$$

with the stress-energy tensor $T_{\mu\nu}$

$$T_{\mu\nu} = g_{\mu\nu}L_s - 2\frac{\partial L_s}{\partial g^{\mu\nu}} \quad (2.7)$$

$$= (\phi_{,\mu}^* \phi_{,\nu} + \phi_{,\nu}^* \phi_{,\mu} + \sigma_{,\mu}^* \sigma_{,\nu} + \sigma_{,\nu}^* \sigma_{,\mu}) - g_{\mu\nu} [\partial_\alpha \phi^* \partial^\alpha \phi + \partial_\alpha \sigma^* \partial^\alpha \sigma + U(|\phi|, |\sigma|)]. \quad (2.8)$$

Variation of (2.5) with respect to the scalar fields leads to the matter equations,

$$\left(\square + \frac{\partial U}{\partial |\phi|^2} \right) \phi = 0, \quad \left(\square + \frac{\partial U}{\partial |\sigma|^2} \right) \sigma = 0, \quad (2.9)$$

where \square represents the covariant d'Alembert operator.

We close this part by noting the existence of several interesting limits of the considered model. First, for a real field ϕ and a choice $\lambda_\sigma = 0$ in the potential (2.2), one recovers the model proposed by Friedberg, Lee and Sirlin (FLS hereafter) in [22], with

$$L_s = \partial_\mu \phi \partial^\mu \phi + \partial_\mu \sigma^* \partial^\mu \sigma + \frac{1}{4} \lambda_\phi (|\phi|^2 - \eta_\phi^2)^2 + \gamma |\phi|^2 |\sigma|^2. \quad (2.10)$$

As shown in [22], this model possesses spherically symmetric, nontopological soliton solutions. In Section 3 we shall give numerical evidence for the existence of spinning, axially symmetric generalizations of those configurations.

Another important limit is found in the special case $\eta_\sigma = \eta_\phi$ by redefining the parameters in the potential as $\lambda_\phi = \lambda_\sigma = \beta$, and $\eta = \frac{1}{2}\beta + \gamma_0$. Then, after taking the limit $\beta \rightarrow \infty$, the theory (2.1) becomes a sigma model for two complex fields ϕ, σ with

$$L_s = \partial_\mu \phi^* \partial^\mu \phi + \partial_\mu \sigma^* \partial^\mu \sigma + \gamma_0 |\phi|^2 |\sigma|^2, \quad (2.11)$$

subject to the constraint

$$|\phi|^2 + |\sigma|^2 = \eta_\phi^2.$$

Note that this model has less degrees of freedom and no free parameters, since the value of γ_0 in (2.11) can be changed by rescaling the spacetime coordinates. Vorton solutions of this model (although for a different formulation) have been discussed in [7].

Finally, one should remark that the system described by (2.5) possesses an interesting limit with $\phi \equiv \eta_\phi$, *i.e.* one scalar field only:

$$L_s = \partial_\mu \sigma^* \partial^\mu \sigma + M_\sigma^2 |\sigma|^2 + \frac{1}{4} \lambda_\sigma |\sigma|^4. \quad (2.12)$$

Different from the above cases, no flat spacetime solitons exist in this case⁴. However, physically interesting solutions are found when gravity is included. These are the gravitating boson stars with a quartic self-interaction potential originally discussed in [23]. The field σ then necessarily possesses a harmonic time dependence (note that the limit $\lambda_\sigma = 0$ is allowed for such solutions). Their existence can be attributed to the balance between the dispersive effect due to the wave character of the complex scalar field and the self-gravitating effect.

2.2 Global charges

Our solutions are globally regular (*i.e.* without an event horizon or conical singularities), and stationary. Also, they approach asymptotically the Minkowski spacetime background. Then their mass M and angular momentum J can be obtained from the respective Komar expressions [24],

$$M = \frac{1}{4\pi G} \int_\Sigma R_{\mu\nu} n^\mu \xi^\nu dV, \quad \mathcal{J} = -\frac{1}{8\pi G} \int_\Sigma R_{\mu\nu} n^\mu \eta^\nu dV. \quad (2.13)$$

Here Σ denotes an asymptotically flat spacelike hypersurface, n^μ is normal to Σ with $n_\mu n^\mu = -1$, dV is the natural volume element on Σ , ξ denotes an asymptotically timelike Killing vector field and η an asymptotically spacelike Killing vector field (corresponding to azimuthal symmetry) [24]. After replacing in (2.13) the Ricci tensor by the stress-energy tensor (via the Einstein equations (2.6)), one finds

$$M = 2 \int_\Sigma \left(T_{\mu\nu} - \frac{1}{2} g_{\mu\nu} T_\gamma{}^\gamma \right) n^\mu \xi^\nu dV, \quad (2.14)$$

$$\mathcal{J} = - \int_\Sigma \left(T_{\mu\nu} - \frac{1}{2} g_{\mu\nu} T_\gamma{}^\gamma \right) n^\mu \eta^\nu dV. \quad (2.15)$$

⁴Here we consider strictly positive values for the parameter λ_σ . However, flat spacetime solitons are found for a potential unbounded from below, $\lambda_\sigma < 0$, in which case they are likely to be unstable.

The Lagrangian (2.1) of the scalar fields has a global $U(1) \times U(1)$ symmetry, $\phi \rightarrow e^{i\alpha_1}\phi$, $\sigma \rightarrow e^{i\alpha_2}\sigma$, which leads to two conserved currents

$$j_{(\phi)}^\mu = -i(\phi^* \partial^\mu \phi - \phi \partial^\mu \phi^*) \ , \quad j_{(\sigma)}^\mu = -i(\sigma^* \partial^\mu \sigma - \sigma \partial^\mu \sigma^*) \ , \quad \text{with} \quad j_{(\phi);\mu}^\mu = 0, \quad j_{(\sigma);\mu}^\mu = 0. \quad (2.16)$$

This implies two conserved Noether charges,

$$Q_{(\phi)} = \int_{\Sigma} j_{(\phi)}^\mu n_\mu dV, \quad Q_{(\sigma)} = \int_{\Sigma} j_{(\sigma)}^\mu n_\mu dV. \quad (2.17)$$

2.3 The axially symmetric ansatz

The line-element for the solutions in this work possesses two commuting Killing vector fields, ξ and η , with

$$\xi = \partial_t \ , \quad \eta = \partial_\varphi, \quad (2.18)$$

in a system of adapted coordinates. General relativity solutions with these symmetries are usually studied within a metric ansatz

$$ds^2 = e^{2U(\rho,z)} \left(e^{2k(\rho,z)} (d\rho^2 + dz^2) + P^2(\rho,z) d\varphi^2 \right) - e^{-2U(\rho,z)} (dt + \Omega(\rho,z) d\varphi)^2, \quad (2.19)$$

where (ρ, z) correspond asymptotically to the usual cylindrical coordinates. In the (electro-)vacuum case, it is always possible to set $P \equiv \rho$, such that only three independent metric functions appear in the equations, and (ρ, z) become the canonical Weyl coordinates [25]. For more general matter sources, however, the generic metric ansatz (2.19) with four independent functions is needed. A variety of interesting general relativity solutions have been constructed within this framework [25], some of them describing toroidal configurations⁵ (see *e.g.* [27, 28]).

One might wonder whether in the numerical study of gravitating ring-shaped solitons other coordinate systems would be better suited. For example, the use of ring coordinates seems to be an obvious choice, since the required symmetry of the configurations is intrinsic in this case. However, even in the absence of back reaction, we have met severe numerical difficulties in the implementation of a numerical scheme for these coordinates⁶.

The solutions in this work are constructed by using ‘quasi-isotropic’ spherical coordinates (r, θ) , defined by the coordinate transformation in (2.19)

$$\rho = r \sin \theta, \quad z = r \cos \theta, \quad (2.20)$$

and possessing the usual range $0 \leq r < \infty$, $0 \leq \theta \leq \pi$. The corresponding line-element⁷ has an ADM-like form and reads

$$ds^2 = \frac{m}{f} (dr^2 + r^2 d\theta^2) + \frac{l}{f} r^2 \sin^2 \theta (d\varphi - \frac{W}{r} dt)^2 - f dt^2. \quad (2.21)$$

The four metric functions f , l , m and W are functions of the variables r and θ only, chosen such that the trivial angular and radial dependence of the line element is already factorized. The relation between the metric functions in the above line-element and those which enter (2.19) is $f = e^{2U} P^2 / (e^{4U} P^2 - \Omega^2)$, $l \sin^2 \theta = P^2$, $m = P^2 / (e^{4U} P^2 - \Omega^2)$ and $W/r = \Omega / (e^{4U} P^2 - \Omega^2)$. The symmetry axis of the spacetime

⁵Note, however, that the known toroidal solutions in four dimensional general relativity do not include black holes. Indeed, for $d = 4$ there are a number of *no go* results forbidding, under very general assumptions, a nonspherical topology of the horizon for an asymptotically flat black hole [26].

⁶For example, the whole of spatial infinity maps in this case to a single point, which leads to bad numerical convergence. Also, the ring radius is an input parameter which should be specified *a priori*; however, this did not appear to be possible within our treatment of the problem.

⁷A similar line element (in particular the same metric gauge choice for the (r, θ) -part of the metric) has also been used in previous numerical work on spinning solutions in general relativity, starting with the early work [29, 30].

is given by $\eta = 0$. It corresponds to the z -axis with $\theta = 0, \pi$. The Minkowski spacetime background is approached for $r \rightarrow \infty$, with $f = l = m = 1$, $W = 0$.

The ansatz for the scalar fields which we shall use is similar to that proposed in the previous work [14], with⁸

$$\phi = X(r, \theta) + iY(r, \theta), \quad \sigma = Z(r, \theta)e^{i(n\varphi + wt)} \quad (2.22)$$

where X, Y, Z are real functions, and w and n are real constants. Single-valuedness of the scalar field σ requires

$$\sigma(\varphi) = \sigma(2\pi + \varphi), \quad (2.23)$$

thus the constant n must be an integer, *i.e.*, $n = 0, \pm 1, \pm 2, \dots$. As usual in the literature, we shall refer to n as rotational quantum number. Without any loss of generality, we shall take in this work $w > 0, n \geq 0$.

We close this part by noting that $\xi = \partial_t$ and $\eta = \partial_\varphi$ are *not* symmetries of the solutions in this work, the system being only *effectively* stationary⁹.

2.4 The equations and the issue of the constraints

After inserting the ansatz (2.21), (2.22) into the field equations (2.6), (2.9) we find a system of seven coupled partial differential equations that needs to be solved. These are four equations for the metric functions f, l, m, W (which are found by taking a suitable combination of the Einstein equations $E_r^r + E_\theta^\theta = 0$, $E_\varphi^\varphi = 0$, $E_t^t = 0$ and $E_\varphi^t = 0$, see Appendix A) and three equations for the functions X, Y and Z describing the scalar fields. The equations are of the form

$$\nabla^2 \mathcal{F}_i = \mathcal{J}_i \quad (2.24)$$

where $\mathcal{F} = (f, l, m, W; X, Y, Z)$, $\nabla^2 = \frac{1}{r^2} \partial_r (r^2 \partial_r) + \frac{1}{r^2 \sin \theta} \partial_\theta (\sin \theta \partial_\theta)$, and \mathcal{J}_i are ‘source’ terms depending on the functions \mathcal{F} and their first derivatives (the explicit form of the equations is presented in Appendix A).

Apart from these, there are two more Einstein equations $E_\theta^r = 0$, $E_r^r - E_\theta^\theta = 0$, which are not solved in practice. Following an argument originally proposed in [35], one can, however, show that the identities $\nabla_\mu E^{\mu r} = 0$ and $\nabla_\mu E^{\mu \theta} = 0$, imply the Cauchy-Riemann relations

$$\partial_{\bar{r}} \mathcal{P}_2 + \partial_\theta \mathcal{P}_1 = 0, \quad \partial_{\bar{r}} \mathcal{P}_1 - \partial_\theta \mathcal{P}_2 = 0, \quad (2.25)$$

with $\mathcal{P}_1 = \sqrt{-g} E_\theta^r$, $\mathcal{P}_2 = \sqrt{-g} r (E_r^r - E_\theta^\theta)/2$ and $d\bar{r} = \frac{dr}{r}$. Therefore the weighted constraints E_θ^r and $E_r^r - E_\theta^\theta$ still satisfy Laplace equations in (\bar{r}, θ) variables. Then they are fulfilled, when one of them is satisfied on the boundary and the other at a single point [35]. From the boundary conditions (2.34)-(2.38) we are imposing, it turns out that this is the case for our solutions, *i.e.* the numerical scheme is consistent.

2.5 Mass, angular momentum and charge

The mass M and the angular momentum J can be evaluated based on the general Komar expressions (2.13). There we insert the metric ansatz (2.21), with unit vector $n = -\sqrt{f} dt$, and volume element $dV =$

⁸Note that (2.22) is not the general ansatz compatible with the symmetries of the line element (2.21). In principle, one can add an extra (r, θ) -dependent phase to the scalar field σ by taking

$$\sigma = |\sigma(r, \theta)| e^{i(\Psi(r, \theta) + n\varphi + wt)} = (Z_1(r, \theta) + iZ_2(r, \theta)) e^{i(n\varphi + wt)}$$

with Z_1, Z_2 real functions. (Solutions with such a complex scalar field were constructed in [14, 34] for a Q-ball model in a fixed Minkowski spacetime background.) Also, one can easily verify that $Z_2 = 0$ is a consistent truncation of the full model.

⁹Thus, one can say that the configurations in this work do not possess Killing vectors. The scalar field σ depends in a nontrivial way on the Killing coordinates φ and t , though the corresponding energy-momentum tensor is still compatible with the spacetime symmetries. This is, however, a generic feature of $d = 4$ gravitating spinning configurations possessing Q-ball features (see also Refs. [31, 32] for examples of $d = 5$ boson stars and black holes with only one Killing vector).

$1/\sqrt{f} \sqrt{-g} dr d\theta d\varphi$. Also, we make use of the fact that both R_t^t and R_φ^t can be expressed as total derivatives:

$$\begin{aligned}\sqrt{-g}R_t^t &= \frac{\partial}{\partial r} \left(r^2 \sin \theta \frac{\sqrt{l}}{2f^2} \left(\sin^2 \theta l W (\partial_r W - \frac{W}{r}) - f \partial_r f \right) \right) + \frac{\partial}{\partial \theta} \left(\sin \theta \frac{\sqrt{l}}{2f^2} (\sin^2 \theta l W \partial_\theta W - f \partial_\theta f) \right), \\ -\sqrt{-g}R_\varphi^t &= \frac{\partial}{\partial r} \left(\frac{r^2 l^{3/2} \sin^3 \theta}{2f^2} (r \partial_r W - W) \right) + \frac{\partial}{\partial \theta} \left(\frac{r l^{3/2} \sin^3 \theta}{2f^2} \partial_\theta W \right),\end{aligned}\quad (2.26)$$

(where $\sqrt{-g} = r^2 \sin \theta \frac{\sqrt{l} m}{f}$). Then it follows that M and J can be read off the asymptotic expansion of the metric functions f and W , respectively

$$f = 1 - \frac{2MG}{r} + O\left(\frac{1}{r^2}\right), \quad W = \frac{2JG}{r^2} + O\left(\frac{1}{r^3}\right), \quad (2.27)$$

i.e. after putting (2.26) into (2.13) one finds

$$M = \frac{1}{2G} \lim_{r \rightarrow \infty} r^2 \partial_r f, \quad J = \frac{1}{2G} \lim_{r \rightarrow \infty} r^2 W. \quad (2.28)$$

Alternatively, the mass M and the angular momentum J can be obtained by direct integration of the expressions (2.14) and (2.15),

$$M = \int_{\Sigma} (2T_\mu^\nu - \delta_\mu^\nu T_\gamma^\gamma) n_\nu \xi^\mu dV = \int (2T_t^t - T_\mu^\mu) \sqrt{-g} dr d\theta d\varphi, \quad (2.29)$$

corresponding to the Tolman mass, and

$$J = - \int T_\varphi^t \sqrt{-g} dr d\theta d\varphi. \quad (2.30)$$

The explicit form of the nonvanishing components of T_μ^ν for the ansatz (2.21), (2.22) is given in Appendix B.

As discussed above, the global $U(1) \times U(1)$ symmetry of the scalar fields may lead to further nonvanishing global charges. For the ansatz of the scalar fields (2.22) with the scalar field ϕ possessing no time dependence, there is only one nonvanishing conserved scalar charge

$$\begin{aligned}Q_{(\sigma)} &= - \int j_{(\sigma)}^t \sqrt{-g} dr d\theta d\varphi \\ &= 4\pi \int_0^\infty dr \int_0^\pi d\theta r^2 \sin \theta \frac{\sqrt{l} m}{f^2} \left(w + n \frac{W}{r} \right) Z^2 = Q.\end{aligned}\quad (2.31)$$

However, one can easily verify that the angular momentum density T_φ^t and the temporal component of the current $j_{(\sigma)}^t$ are proportional, $T_\varphi^t = n j_{(\sigma)}^t$. Then, from Eq. (2.30) for the angular momentum J and Eq. (2.31) for the scalar charge Q , one obtains the important quantization relation for the angular momentum,

$$J = n Q. \quad (2.32)$$

Thus Q is not an independent global charge, and the vortons' angular momentum is carried by the scalar field σ only. Also, it follows that all solutions with $J \neq 0$, thus in particular the vorton solutions, cannot be viewed as perturbations around some static configurations¹⁰. (Note, that (2.32) holds for solutions in a flat spacetime background as well.)

We close this part by noting that gravitating vortons have no horizon. Therefore they are zero entropy objects, without an intrinsic temperature. The first law of thermodynamics [33] reads in this case

$$dM = w dQ = \frac{w}{n} dJ. \quad (2.33)$$

¹⁰ A similar result has been found for Q-balls and boson star solutions [29, 17, 30].

2.6 Boundary conditions

In our approach, the solutions are constructed by solving the set (A.1)-(A.6) of seven elliptic partial differential equations supplemented with suitable boundary conditions on the boundaries of the domain of integration (see the discussion in Section 2.8). The choice of appropriate boundary conditions must guarantee that the solutions are globally regular and asymptotically flat, and that they possess finite global charges with finite densities¹¹.

Thus, at the origin $r = 0$ we require

$$\partial_r f|_{r=0} = \partial_r l|_{r=0} = \partial_r m|_{r=0} = W|_{r=0} = 0, \quad \partial_r X|_{r=0} = Y|_{r=0} = Z|_{r=0} = 0, \quad (2.34)$$

The boundary conditions at infinity are such that the ground state of the model is approached,

$$f|_{r \rightarrow \infty} = l|_{r \rightarrow \infty} = m|_{r \rightarrow \infty} = 1, \quad W|_{r \rightarrow \infty} = 0, \quad X|_{r \rightarrow \infty} = \eta_\phi, \quad Y|_{r \rightarrow \infty} = Z|_{r \rightarrow \infty} = 0. \quad (2.35)$$

On the symmetry axis ($\theta = 0$ and $\theta = \pi$), we require the boundary conditions

$$\partial_\theta f|_{\theta=0,\pi} = \partial_\theta l|_{\theta=0,\pi} = \partial_\theta m|_{\theta=0,\pi} = \partial_\theta W|_{\theta=0,\pi} = 0, \quad \partial_\theta X|_{\theta=0,\pi} = \partial_\theta Y|_{\theta=0,\pi} = Z|_{\theta=0,\pi} = 0. \quad (2.36)$$

The elementary flatness condition [25] (*i.e.* the absence of conical singularities) imposes an extra condition on the symmetry axis

$$l|_{\theta=0,\pi} = m|_{\theta=0,\pi}. \quad (2.37)$$

The solutions in this work possess an extra symmetry *w.r.t.* reflection in the equatorial plane $z = 0$ ($\theta = \pi/2$). Namely, all functions except Y are invariant under the transformation $\theta \rightarrow \pi - \theta$, while Y changes the sign. We use this symmetry to reduce the domain of integration to $[0, \infty) \times [0, \pi/2]$. Then the boundary conditions which are imposed in the equatorial plane are

$$\partial_\theta f|_{\theta=\pi/2} = \partial_\theta l|_{\theta=\pi/2} = \partial_\theta m|_{\theta=\pi/2} = \partial_\theta W|_{\theta=\pi/2} = 0, \quad \partial_\theta X|_{\theta=\pi/2} = Y|_{\theta=\pi/2} = \partial_\theta Z|_{\theta=\pi/2} = 0. \quad (2.38)$$

2.7 Scaling properties and input parameters

A simple inspection of the field equations reveals that the model possesses seven input parameters: $\{\lambda_\phi, \lambda_\sigma, \eta_\phi, \eta_\sigma, \gamma\}$ and $\{w, n\}$. However, as usual, some of them can be absorbed into a redefinition of variables together with suitable rescalings.

Let us start with the simplest case of nongravitating solutions. Then the scaling of the fields

$$\phi \rightarrow \eta_\phi \phi, \quad \sigma \rightarrow \eta_\phi \sigma \quad (2.39)$$

together with the redefinitions

$$\lambda_\phi \rightarrow \lambda_\phi / \eta_\phi^2, \quad \lambda_\sigma \rightarrow \lambda_\sigma / \eta_\phi^2, \quad \gamma \rightarrow \gamma / \eta_\phi^2, \quad (2.40)$$

show that one can set $\eta_\phi = 1$ in all field equations without loss of generality. Then η_ϕ^2 appears as an overall factor in front of the (rescaled-) Lagrangian density.

In the next step, we note that a rescaling of the spacetime coordinates

$$x^\mu \rightarrow x^\mu / L \quad (2.41)$$

(with $L > 0$ an arbitrary constant) together with a redefinition of several parameters in the potential

$$\lambda_\phi \rightarrow \lambda_\phi L^2, \quad \lambda_\sigma \rightarrow \lambda_\sigma L^2, \quad \gamma \rightarrow \gamma L^2, \quad (2.42)$$

¹¹These boundary conditions are also implied by a power series expansion of the solutions on the boundaries of the domain of integration.

leaves the field equations invariant. This symmetry is used in this work to set¹² the length scale of the vortons as given by the mass of the scalar field ϕ ,

$$L = \frac{1}{M_\phi} = \frac{1}{\eta_\phi \sqrt{\lambda_\phi}}. \quad (2.43)$$

This directly reveals the existence of three essential, dimensionless parameters of the nongravitating vorton model

$$\beta_1 = \frac{\eta_\sigma}{\eta_\phi}, \quad \beta_2 = \frac{\lambda_\sigma}{\lambda_\phi}, \quad \beta_3 = \frac{\gamma}{\lambda_\phi}. \quad (2.44)$$

From (2.3), the parameters β_i should satisfy the conditions

$$4\beta_3^2 > \beta_2, \quad \beta_3 > \frac{1}{2}\beta_2\beta_1^2. \quad (2.45)$$

Note that the scalings above are independent of any ansatz. However, when considering a scalar σ of the form (2.22), one has to take also

$$w \rightarrow w/M_\phi, \quad (2.46)$$

such that the phase of σ remains invariant under the scaling (2.41), with L given by (2.43).

The scalings discussed above hold also when gravity is included. However, in that case, the presence of Newton's constant G leads to the occurrence of one more dimensionless coupling constant, which, following previous work on solitons coupled to gravity [21], we shall call α , with

$$\alpha^2 = 16\pi G \eta_\phi^2. \quad (2.47)$$

Thus the constant α corresponds to the ratio between the symmetry breaking scale and the Planck mass $M_{Pl} = 1/\sqrt{G}$. On general grounds, we expect this ratio to be very small; however, to understand the general pattern of the solutions, we shall attempt to investigate the full range of α .

Then, for the specific ansatz (2.21), (2.22) with the above scalings, the equations for gravitating vortons (which are effectively solved) can be derived by extremizing the following reduced action

$$S_{red} = \int dr d\theta (\mathcal{L}_g - \alpha^2 \mathcal{L}_s), \quad (2.48)$$

with (here we define $(\nabla A) \cdot (\nabla B) = A_{,r} B_{,r} + \frac{1}{r^2} A_{,\theta} B_{,\theta}$):

$$\begin{aligned} \mathcal{L}_g &= r^2 \sin \theta \sqrt{l} \left[\frac{1}{2lm} (\nabla l) \cdot (\nabla m) + r^2 \sin \theta \frac{l}{2f^2} (\nabla W)^2 - \frac{1}{2f^2} (\nabla f)^2 \right. \\ &\quad \left. - \frac{1}{rl} (l_{,r} + \frac{\cot \theta}{r} l_{,\theta}) + \frac{1}{rm} (m_{,r} + \frac{\cot \theta}{r} m_{,\theta}) \right], \\ \mathcal{L}_s &= r^2 \sin \theta \frac{m\sqrt{l}}{f} \left[\frac{f}{m} ((\nabla X)^2 + (\nabla Y)^2 + (\nabla Z)^2) + \frac{1}{4} (X^2 + Y^2 - 1)^2 + \frac{\beta_2}{4} Z^2 (Z^2 - 2\beta_1^2) \right. \\ &\quad \left. + \beta_3 Z^2 (X^2 + Y^2) - \frac{1}{f} (w + \frac{nW}{r})^2 Z^2 + \frac{n^2}{r^2 \sin^2 \theta} \frac{f}{l} Z^2 \right]. \end{aligned} \quad (2.49)$$

In the above relations we use a dimensionless radial variable r and a dimensionless frequency w given in units set by M_ϕ . These conventions we shall use for all numerical data reported in this work. Also, in all plots, the total mass M is given in units of $4\pi M_\phi/\lambda_\phi$, while the total angular momentum J and the charge Q are given in units of $4\pi/\lambda_\phi$. The components T_t^t and T_φ^φ of the energy momentum tensor are given in units of M_ϕ^4/λ_ϕ and M_ϕ^3/λ_ϕ , respectively.

¹²Note that other choices are possible. For example, one can also set $L^2 = 1/\lambda_\sigma \eta_\phi^2$ or $L^2 = 1/\gamma \eta_\phi^2$. However, the choice (2.43) leads to a length scale with a transparent physical meaning.

2.8 The numerical method

The set of seven coupled non-linear elliptic partial differential equations for the functions $\mathcal{F} = (X, Y, Z; f, l, m, W)$ has been solved numerically subject to the boundary conditions (2.34)-(2.38). In a first stage, a new compactified radial variable x is introduced instead of r , such that the semi-infinite region $[0, \infty)$ is mapped to the finite interval $[0, 1]$. (This avoids the use of a cutoff radius.) There are various possibilities for such a mapping, a flexible enough choice being $x = r/(1 + r)$. This involves the following substitutions in the differential equations

$$r\mathcal{F}_{,r} \longrightarrow (1-x)\mathcal{F}_{,x} \quad \text{and} \quad r^2\mathcal{F}_{,rr} \longrightarrow (1-x)^2\mathcal{F}_{,xx} - 2(1-x)\mathcal{F}_{,x}. \quad (2.50)$$

Next, the equations for these functions are discretized on a grid in x and θ . Here we have considered various grid choices, the number of grid points ranging between 280×30 and 150×70 . The grid covers the integration region $0 \leq x \leq 1$ and $0 \leq \theta \leq \pi/2$.

All numerical calculations have been performed by using the professional package FIDISOL/CADSOL [36]. This code requests the system of nonlinear partial differential equations in the form $P(x, \theta; \mathcal{F}; \mathcal{F}_x, \mathcal{F}_\theta; \mathcal{F}_{x\theta}, \mathcal{F}_{xx}, \mathcal{F}_{\theta\theta}) = 0$, subject to a set of boundary conditions on a rectangular domain. Besides that, FIDISOL/CADSOL requires the Jacobian matrices for the equations *w.r.t.* the functions \mathcal{F} and their first and second derivatives, the boundary conditions, as well as some initial guess for the functions \mathcal{F} . The solver uses a Newton-Raphson method, which requires to have a good first guess in order to start a successful iteration procedure. This software package provides also error estimates for each function, which allows to judge the quality of the computed solution. The typical numerical error¹³ for the solutions reported in this work is estimated to be of the order of 10^{-3} . A detailed description of the numerical method and explicit examples are provided in [36] (see also *e.g.* the Appendix in [37] for a discussion within a physical problem). As a further check of numerics, we have verified that the families of solutions with a varying frequency satisfy with a very good accuracy the first law of thermodynamics (2.33).

In this scheme, there are six input parameters: the parameters β_i in the potential of the scalar fields, the (scaled) frequency w and the winding number n in the ansatz for the scalar field σ , and also the constant α as given by (2.47). The number of nodes k of $|\phi|$ in the equatorial plane (which provides a classification of the solutions, see the discussion below), as well as the global charges (mass and angular momentum) are computed from the numerical solution.

In constructing gravitating solutions, we start with flat spacetime configurations as initial guess (*i.e.* taking $f = l = m = 1$, $W = 0$). Then we slowly increase the value of α . When the iterations converge we obtain, by repeating this procedure, solutions for higher values of α . A similar procedure is used to investigate the dependence on other parameters of the problem, starting instead with solutions with a given α . Also, in some of the calculations, we interpolate the resulting configurations on points between the chosen grid points, and then use these for a new guess on a finer grid.

As a general remark, we have found the study of vortons more difficult than a number of other problems which we studied with a similar approach. First, the present system possesses a large parameter space, and the solutions exist only in some regions there (and thus not for arbitrary values of $\{\beta_i, w, n, \alpha\}$). Moreover, rather good initial profiles are usually required for the convergence of the numerical iteration. Next, the profiles of the scalar functions exhibit large gradients in a small region around the equatorial plane, which requires a careful choice of the grid. Finally, the problem is further complicated by the possible existence of several different solutions for the same input parameters (see the discussion below).

3 Solutions in flat space: nongravitating vortons

3.1 The heuristic construction of a vorton and general features

As mentioned in the introduction, vortons are essentially loops made of pieces of vortices. Remarkably, this simple heuristic construction leads to a number of predictions about their qualitative properties. This is why

¹³However, the errors increase dramatically when studying solutions close to the limits of the domain of existence in the parameter space.

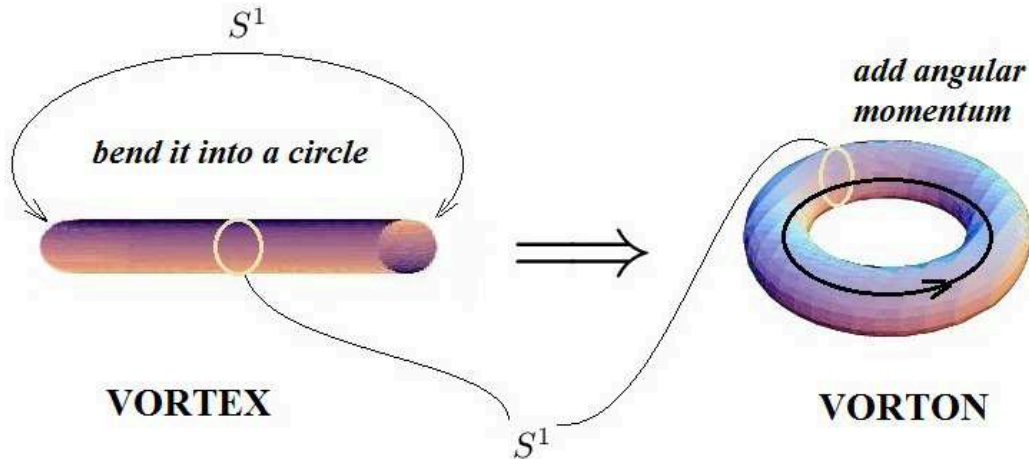


Figure 2. The heuristic construction of a vorton starting with a piece of a vortex.

we shall start with a discussion of this point (more details on that, including relevant plots, are given in Section 6 of Ref. [14]).

As discussed by several authors (see *e.g.* [2, 38, 39]), Witten's model of superconducting strings admits cylindrically symmetric, vortex-type solutions. For a cylindrically symmetric line element with $ds^2 = d\rho^2 + \rho^2 d\psi^2 + dz^2 - dt^2$, the appropriate ansatz for the scalar fields reads

$$\phi = |\phi(\rho)|e^{ik\psi}, \quad \sigma = |\sigma(\rho)|e^{i(k_z z - wt)}. \quad (3.51)$$

As usual, the single-valuedness of the scalar fields imposes k to be an integer, $k = 0, \pm 1, \dots$, while there are no apriori restrictions for k_z, w in (3.51).

A study of the asymptotic form of the solutions reveals that the scalar field ϕ approaches the vacuum expectation value (*v.e.v.*) for $\rho \rightarrow \infty$; as $\rho \rightarrow 0$, $|\phi|$ behaves as ρ^k (thus it vanishes on the z -axis, unless $k = 0$). At the same time, σ is always nonzero at $\rho = 0$ (where $|\sigma|$ takes its maximal value) and vanishes as $\rho \rightarrow \infty$. (This is why ϕ and σ are usually referred to as vortex and condensate fields, respectively.) Then the phase of ϕ changes by $2\pi k$ after one revolution around the vortex, while the phase of σ increases along the vortex.

Solutions with this behaviour can be constructed by using a standard ordinary differential equations solver; typical profiles for $|\phi|$, $|\sigma|$ and a discussion of their basic properties can be found in [38]. These configurations possess a nonzero momentum along the vortex, with $T_z^t = k_z w |\sigma|^2$. Also, their energy density is finite everywhere. However, for $k \neq 0$, the total mass per unit length exhibits a logarithmic divergence originating in the ϕ -sector of the model¹⁴.

The heuristic construction of a vorton involves taking a piece of length L of such a vortex and identifying its ends to make a loop (see Figure 2). Therefore the central axis of the vortex where the field ϕ vanishes (for $k \neq 0$), becomes a circle of radius $R = L/2\pi$. Then the coordinate z along the vortex becomes periodic, being replaced by the azimuthal angle φ . This implies that the constant k_z in (3.51) also becomes quantized, $k_z = 2\pi n/L$. In such a heuristic construction, the momentum T_z^t along the vortex will then circulate along the loop, thus implying a nonzero angular momentum density. Then the corresponding centrifugal force will compensate the tension of the loop, thereby producing an equilibrium configuration.

The vorton would inherit some basic properties of the initial vortex configuration. For example, for $k \neq 0$, the magnitude of the field ϕ would vanish on a circle of radius R in the equatorial plane (the initial position of the vortex). At the same time, the maxima of the condensate scalar field σ would be located on the same circle at $\theta = \pi/2$. Also, it is clear that a configuration generated in this way would possess an intrinsic toroidal symmetry, the angle ψ for the vortex becoming an S^1 generator of the resulting torus, see Figure 2.

¹⁴Note that this divergence is cured when the ϕ -field is gauged.

Based on this heuristic construction, a description of large radius vortons has been proposed in [10], within an approximation of the vortons' cross section by that of an infinite string carrying a current¹⁵.

From the above analysis, it is clear that the resulting toroidal configurations can be described by the following axially symmetric ansatz,

$$\phi = |\phi(r, \theta)|e^{i\psi_1(r, \theta)} = X(r, \theta) + iY(r, \theta), \quad \sigma = |\sigma(r, \theta)|e^{i(n\varphi + wt)} = Z(r, \theta)e^{i(n\varphi + wt)}. \quad (3.52)$$

Then any axially symmetric vorton configuration can be characterized by a pair of integers. Apart from the azimuthal winding number n which enters the ansatz (3.52) explicitly, they inherit¹⁶ also the integer k of the initial vortex configuration (3.51). This can be seen as follows: the amplitude of the scalar field ϕ should vanish for some value of r at $\theta = \pi/2$, while its phase twists by $2\pi k$ after one revolution around the boundary of the half-plane consisting of the z -axis (with $z = r \cos \theta$) and a half-circle at infinity.

Then, following [14], one can formally define a 'topological charge', which is the product of the two integers characterizing the $S^1 \times S^1$ topology of the torus

$$N = nk. \quad (3.53)$$

However, one should emphasize that, for the model considered in this paper, the solutions do not describe topological solitons and thus (3.53) is not a topologically invariant quantity. $N = nk$ becomes a topological charge only in the sigma-model limit (2.11) (see Ref. [7]).

Unfortunately, in the absence of exact solutions, it is extremely difficult to follow the details of the above heuristic construction¹⁷. Moreover, while the numerical construction of the initial vortices does not pose special problems (since one deals with ordinary differential equations), the systematic study of vortons represents a numerical challenge¹⁸. An approximate form of the solutions can be found on the boundaries of the domain of integration only. For example, the leading terms in the asymptotic form of the solutions, as $r \rightarrow \infty$, read (restoring the dimensionful variables)

$$\psi_1 = \frac{A \sin \theta}{r^2} + \dots, \quad |\phi| = 1 - \frac{1}{\eta_\phi \lambda_\phi} \frac{A^2}{r^6} (1 + 3 \cos^2 \theta) + \dots + \frac{C}{r} e^{-M_\phi r} + \dots, \quad |\sigma| = \frac{B}{r} e^{-\sqrt{M_\sigma^2 - w^2} r} + \dots, \quad (3.54)$$

with $X = |\phi| \cos \psi_1$, $Y = |\phi| \sin \psi_1$ and A, B, C arbitrary constants. Note, that finiteness of the mass imposes an upper bound on the frequency,

$$w^2 < w_{max}^2 = \gamma \eta_\phi^2 - \frac{1}{2} \lambda_\sigma \eta_\sigma^2 = M_\sigma^2. \quad (3.55)$$

When expressed in terms of the dimensionless parameters, the above condition reads

$$\beta_3 > w^2 + \frac{1}{2} \beta_2 \beta_1^2, \quad (3.56)$$

a form which helps to understand the critical behaviour of the numerical solutions.

Also, as proven in [14], vortons in a flat spacetime background satisfy the virial identity

$$\mathcal{T} + \mathcal{U} = \frac{3w}{2} Q \quad (3.57)$$

with¹⁹

$$\mathcal{T} = \int d^3x (|\nabla \phi|^2 + |\nabla \sigma|^2), \quad \mathcal{U} = \int d^3x U(|\phi|, |\sigma|), \quad Q = 2w \int d^3x |\sigma|^2, \quad (3.58)$$

¹⁵However, as discussed in [18], this approximation fails to provide a good quantitative description, at least for the vorton solutions investigated in that work. This is presumably due to the fact that the initial vortices have an infinite energy per unit length. However, a similar description of large radius vortons provides excellent agreement with the full numerical simulation for $d = 2 + 1$ dimensions [42].

¹⁶Note, that the number k can be defined also for non-axially symmetric configurations.

¹⁷Remarkably, a similar heuristic construction could be demonstrated in $d = 5$ Einstein gravity [41]. The large radius black rings there are essentially boosted black strings.

¹⁸The correspondence between vortices and vortons could be studied in detail for planar *kinky* vortons, *i.e.* solutions in $2 + 1$ dimensions [42]. The starting configuration represents a kink string, which is known in closed form. This leads to a number of exact results and greatly simplifies both the analytical and numerical treatment of the problem.

¹⁹Here the operator ∇ is expressed with respect to the three dimensional euclidean metric.

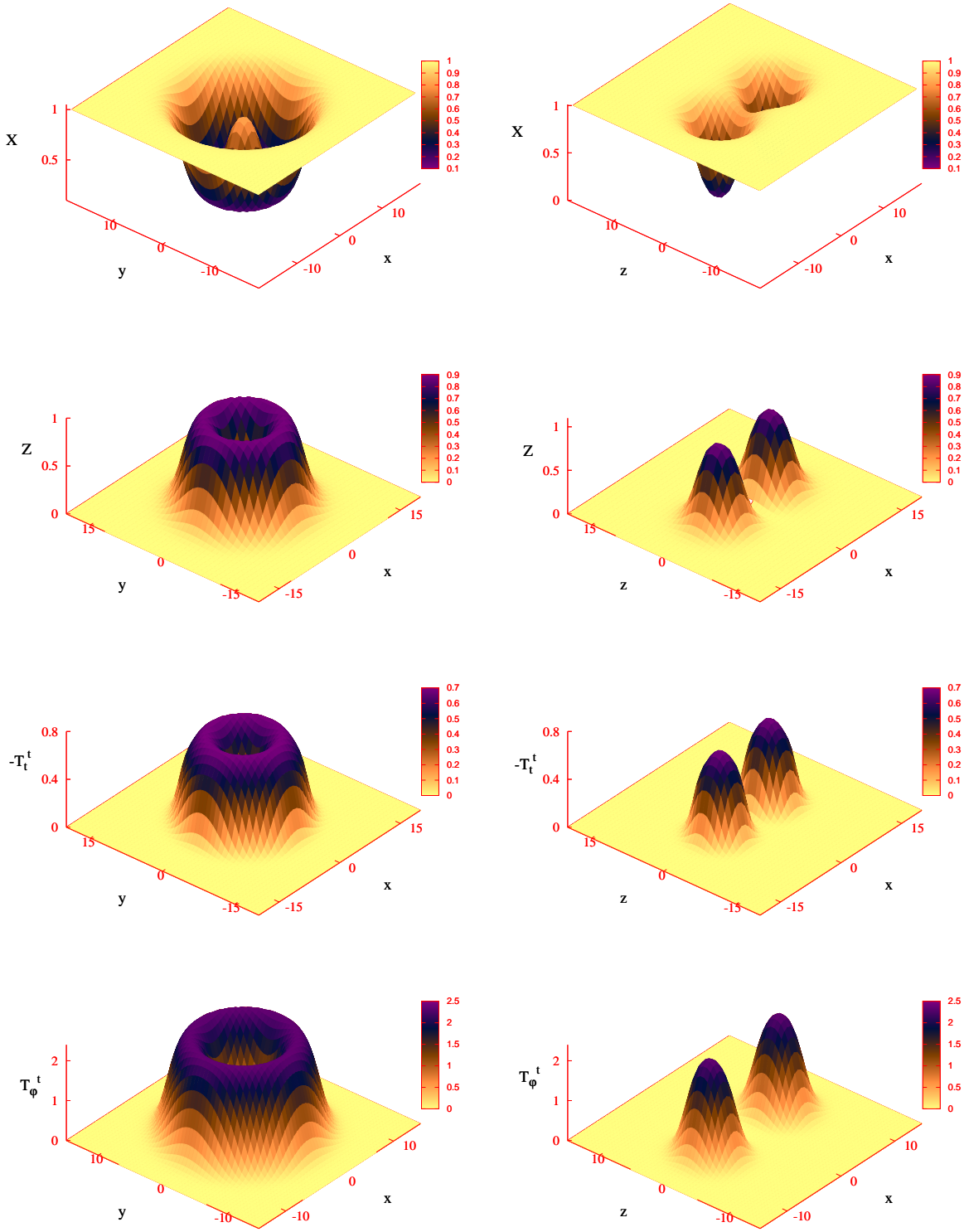


Figure 3. The scalar functions X , Z , the energy density $-T_t^t$ and the angular momentum density T_ϕ^t are shown for a typical $k = 0$ ‘semitopological’ vorton. The left plots are for the $z = 0$ plane, while the right plots are for a plane containing the axis of symmetry. The parameters of the solution are $w = 0.75$, $n = 2$ and $\beta_1 = 0.71$, $\beta_2 = 2.22$, $\beta_3 = 1.7$.

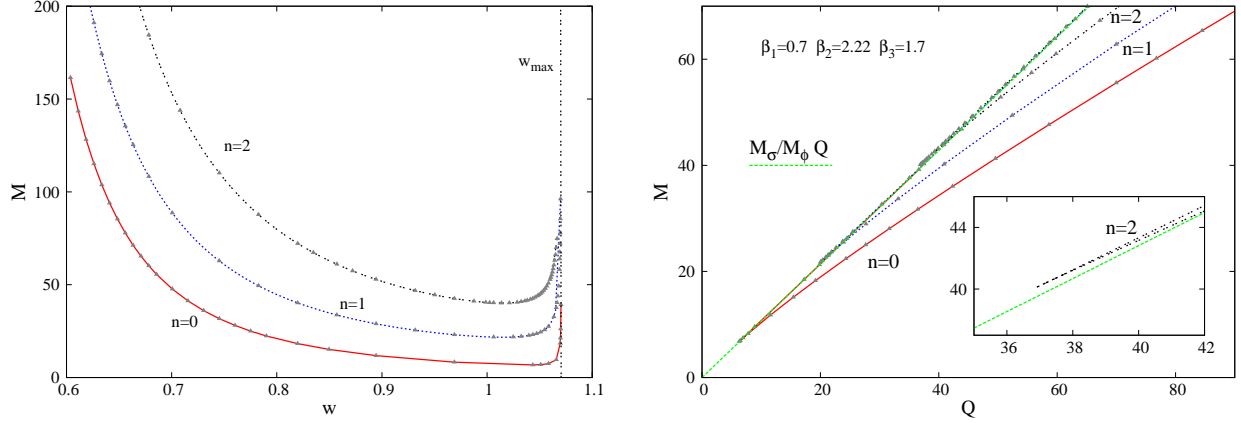


Figure 4. *Left:* The mass of $k = 0$ ‘semitopological’ vortons in a flat spacetime background is shown as a function of the frequency for several values of the azimuthal winding number n . The vertical line corresponds to the maximal value of the frequency as given by (3.55). *Right:* The $M(Q)$ diagram for the same solutions. Also shown is the mass for Q free bosons, $M = M_\sigma/M_\phi Q$ as given in units set by the scalar field ϕ . Note, that in all figures in this work exhibiting results for families of solutions, the large dots represent the data points.

which clearly shows that the solutions owe their existence to the harmonic time dependence of the condensate field σ . Note, that (3.57) holds for generic solutions of the model, without any symmetry assumption. The mass of the solutions can be written in terms of the above quantities as

$$M = \mathcal{T} + \frac{1}{2}wQ + \mathcal{U}.$$

For spinning axially symmetric solutions, a more suggestive form of (3.57) is found by replacing $Q = J/n$. Then one can see that the angular momentum of the solutions is bounded from below, *i.e.* the limit $J \rightarrow 0$ is not allowed. The relation (3.57) is also used to verify the accuracy of the numerical results.

A rather similar virial identity holds for Q -ball solutions [14]. These are solitonic solutions in a model with a single complex scalar field which vanishes at infinity (like σ) and possesses a non-renormalizable potential. This suggests to view the toroidal solutions as ϕ -dressed Q -balls made of the complex σ -field, where the non-renormalizable $|\sigma|^6$ term in the Q -ball potential is replaced by the interaction with the scalar field ϕ . As we shall see, the numerical results give some support for this analogy. However, the vortons possess also some special features which singularize them.

3.2 $k = 0$ ‘semitopological’ vortons

These are the simplest solutions of the model studied in this work. In a heuristic construction, they are found by starting with loops made of vortices possessing $k = 0$ in the vortex ansatz (3.51). This implies that the scalar field ϕ is purely real, *i.e.* $Y \equiv 0$.

Moreover, since ϕ does not vanish at the core of the vortex, then, for the corresponding axially symmetric solution, X should be a nodeless function²⁰.

The azimuthal winding number n is non-trivial in this case, but the ‘topological charge’ $N = kn$ as defined by (3.53) is zero, and so strictly speaking these solutions should not be called vortons. Then in what follows we shall call these configurations ‘semitopological’ vortons.

Also, in some sense they represent axially symmetric generalizations²¹ of the spherically symmetric

²⁰Indeed, for all solutions with a real ϕ which we could construct, the function $X(r, \theta)$ was strictly positive.

²¹The FLS model [22] is recovered for a vanishing σ -potential in (2.2). However, we have found that the basic properties of the more general solutions here hold also in that limit.

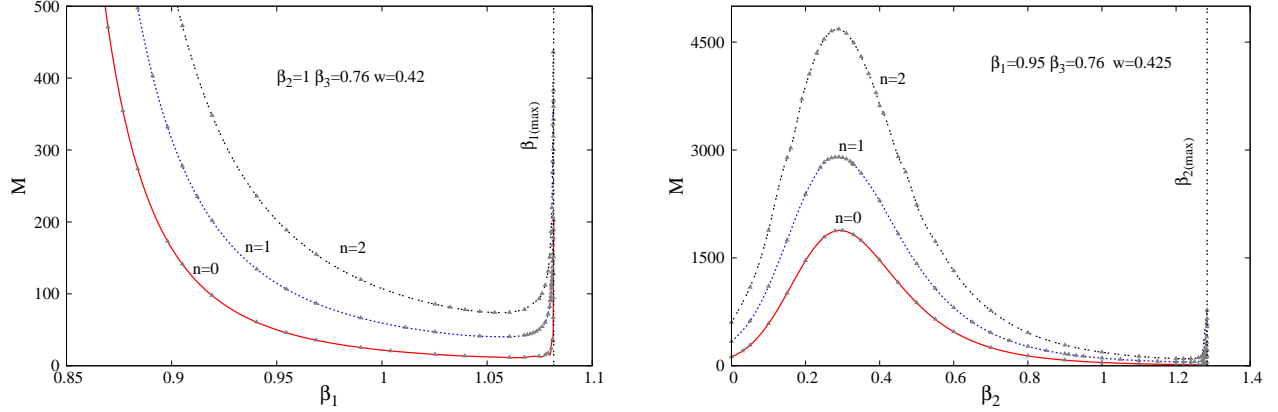


Figure 5. The dependence of the $k = 0$ solutions on the parameters β_1 , β_2 is shown for several values of the winding number n .

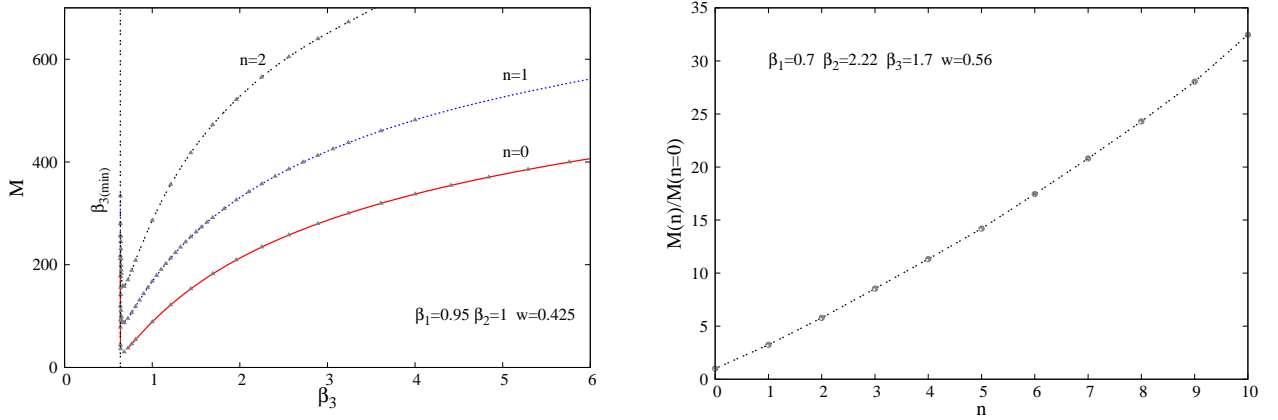


Figure 6. *Left:* The dependence of the $k = 0$ solutions on the parameter β_3 , is shown for several values of the winding number n . Here and in Figure 5, the vertical lines correspond to the limiting values of β_i as given by (3.56). *Right:* The mass of typical $k = 0$ vorton solutions is shown as a function of the azimuthal winding number n for fixed parameters of the potential and a given frequency.

solitons studied by Friedberg, Lee and Sirlin in [22].

For $n \neq 0$, the $k = 0$ configurations satisfy the same boundary conditions as in (2.34), (2.35), (2.36), (2.38) (with $Y \equiv 0$ this time). The profiles of a typical solution are shown in Figure 3, together with the corresponding distributions for the energy density $-T_t^t$ and the angular momentum density T_φ^t . There we plot the quantities for a slice corresponding to the $z = 0$ plane (left panel) and also for the $y = 0$ plane (with x, y, z the usual cartesian coordinates).

One can see that the functions X, Z possess a pronounced angular dependence, with a nonzero minimum of X located in the $\vartheta = \pi/2$ plane ($z = 0$), at some value $r = R$. There the function Z approaches the maximal value, and likewise the energy and angular momentum densities. Based on that, we can define formally an effective ring radius R also for the $k = 0$ solutions²². The energy density typically exhibits a

²²Alternatively, following [40] one can define a mean radius of the configurations $R = \frac{\int r j_{(\sigma)}^t \sqrt{-g} d^3 x}{\int j_{(\sigma)}^t \sqrt{-g} d^3 x}$.

torus-like structure. (This becomes apparent by considering surfaces of constant energy density of *e.g.* half the respective maximal value of the energy density.)

Here we note that the $k = 0$ configurations are obtained easily, and with a better numerical accuracy than any other solutions in this work. Therefore it was possible to investigate some regions of the five-dimensional parameter space in a systematic way. Starting with the dependence on the frequency, we note that the behaviour found in [16] for flat spacetime spinning Q-ball solutions is recovered, see Figure 4. (Similar results have been found also for other sets of input parameters.) As one can see, the solutions exist for a limited range of frequency, $w_{min} < w < w_{max}$ (with $w_{max} = M_\sigma/M_\phi$ for the scaling used in this work, see (3.56)). Both mass and charge (or, equivalently $J = nQ$) diverge at the limits of this interval. They assume minimal values at some intermediate value w_{cr} . Then a diagram $M(Q)$ shows the existence of two branches, see Figure 4 (right). For the same Q , the solution with $w < w_{cr}$ has lower mass than the corresponding one with $w > w_{cr}$. Moreover, those configurations which have a smaller mass than a collection of non-interacting field quanta with the same charge are expected to be stable with respect to decay to the free particles²³, at least for small values of n .

The dependence of the solutions on the parameter β_1 is exhibited in Figure 5 (left). One can see that the solutions exist only for a limited interval, $\beta_{1(min)} < \beta_1 < \beta_{1(max)}$, and the mass diverges as the limits are approached. Interestingly, the value of $\beta_{1(max)}$ does not depend on the winding number n , with $\beta_{1(max)} = \sqrt{2(\beta_3 - w^2)/\beta_2}$, see the relation (3.56).

When studying instead the dependence on β_2 , one first notices the existence of axially symmetric generalizations of the FLS spherically symmetric solitons [22], which are found for $\beta_2 \rightarrow 0$. Also, the mass seems to diverge when a critical, maximal value of β_2 is approached, see Figure 5 (right). As implied by (3.56), this maximal value is given by $2(\beta_3 - w^2)/\beta_1^2$ (and thus again it does not depend on n).

We have performed a similar study also for β_3 , see Figure 6 (left). One can notice the existence of a minimal value of this parameter, $\beta_{3(min)} = w^2 + \frac{1}{2}\beta_2\beta_1^2$, see (3.56). As $\beta_3 \rightarrow \beta_{3(min)}$ the mass diverges. At the same time, no upper bound on β_3 appears to exist, at least for the set of parameters we have considered. Finally, in Figure 6 (right), we plot the dependence of mass on the winding number n (where one can notice an almost linear relation). Also, as expected, the angular dependence of the scalar functions increases with the winding number n and the location of the biggest angular splitting moves further outward, as well as the global maximum of the energy density.

Note also that for all cases in Figures 5, 6, the charge Q shows a similar pattern. (Here we recall that in all plots in this work the global charges are expressed in natural units set by η_ϕ, λ_ϕ .)

The $k = 0$ solutions possess also an interesting spherically symmetric limit, in which case $n = 0$ and $X(r, \theta) = X(r)$ and $Z(r, \theta) = Z(r)$ (with $Z(0) \neq 0$ this time). Some properties of these static solutions are discussed in a more general context in Appendix C. Here we mention that, as seen in Figures 4-6, they share the basic properties of the spinning solutions.

We close this part by remarking that since the study of the $k = 0$ solutions does not pose special numerical difficulties, and also the corresponding vortices possess a finite mass per unit length, these may open the possibility to work out the details of the heuristic construction described in Section 3.1. We hope to report elsewhere on that.

3.3 $k = 1$ vortons

The distinguishing feature of these solutions is that the vortex field ϕ has a zero on a circle in the $\theta = \pi/2$ plane (*i.e.* at $z = 0$). The profiles of a typical solution are shown in Figure 7. There the plots are again given for the (xy) and (xz) planes. (Note, that the $X, Y, Z, |\phi|$ profiles are shown in Figure 15 in terms of cylindrical coordinates (ρ, z) .) We also recall that x, y, z correspond to dimensionless coordinates, the length scale being set by $1/M_\phi$.

A description of the generic properties of the scalar functions can be made as follows. At $r = 0$, Z vanishes, while X has a local (negative) extremum. Near the origin, the functions X, Y, Z show a large

²³This conjecture is based also on similarities we have found between the $k = 0$ solutions and the spinning Q-balls in a model with a single complex scalar field. In that case, as discussed in [43] (though for a different formulation of the problem), the $n = 0, 1$ solitons are stable for some range of frequency, both at the linear and non-linear levels.

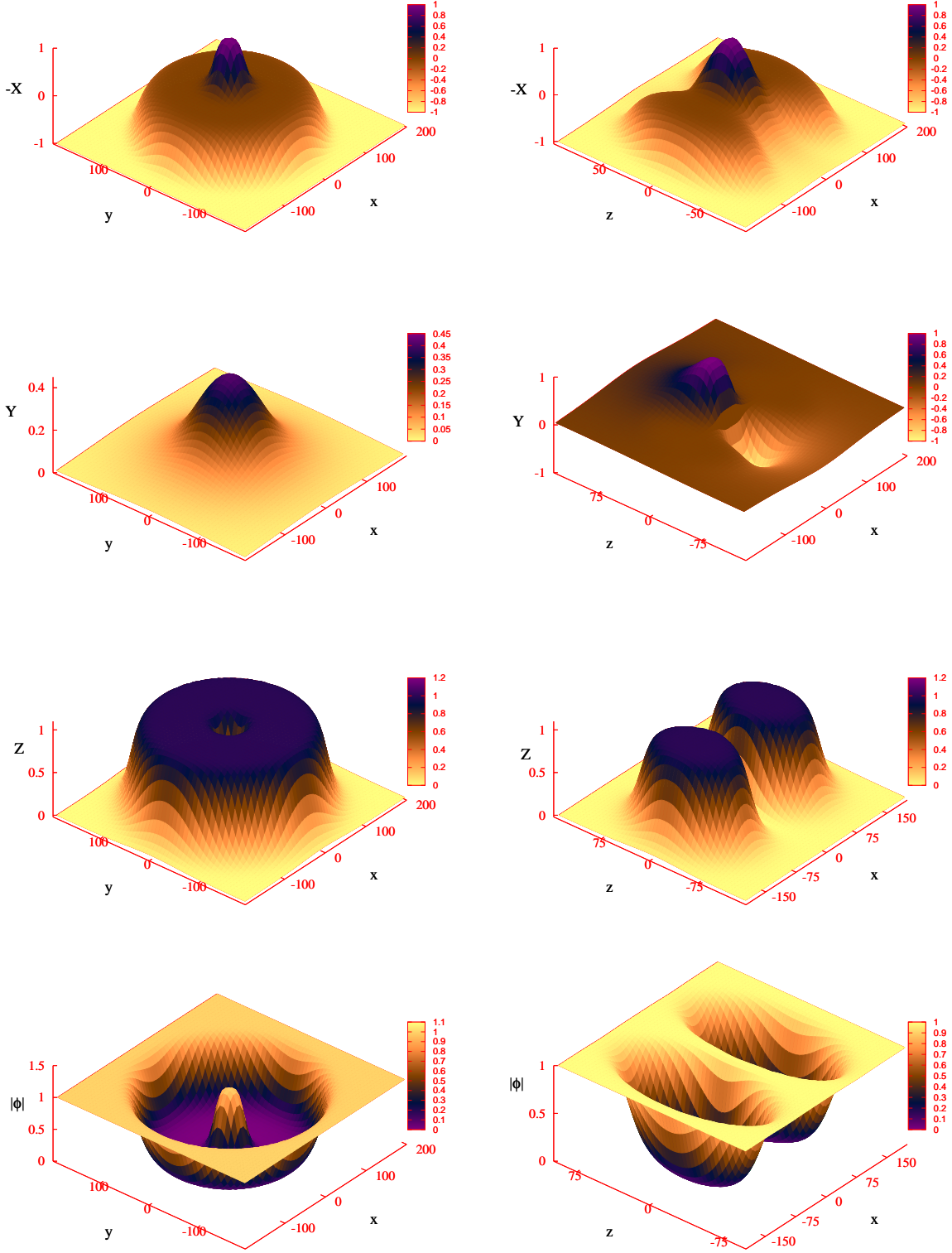


Figure 7. The scalar functions X , Y , Z and the amplitude $\sqrt{X^2 + Y^2}$ of the field ϕ are shown for a typical $k=1$ vorton solution.

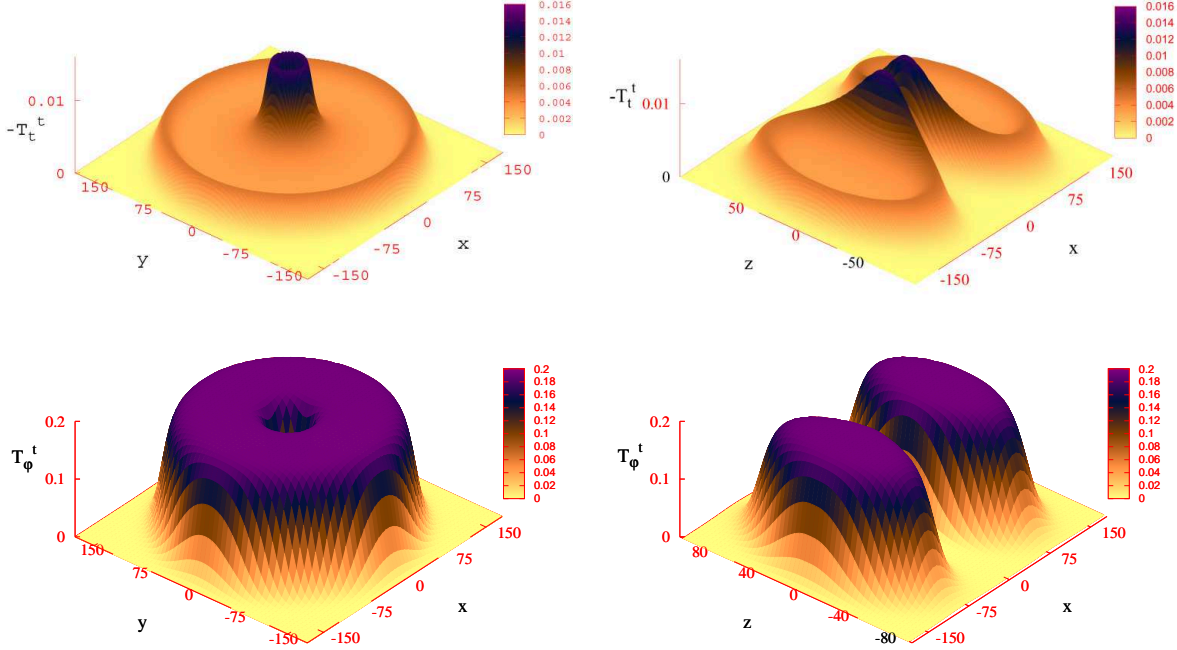


Figure 8. The energy density $-T_t^t$ and the angular momentum density T_ϕ^t are shown for the same solution in Figure 7. The input parameters of the solution are $w = 0.05$, $n = 2$ and $\beta_1 = \beta_2 = 1$, $\beta_3 = 0.51$. Here and in Figure 7, the left plots are for the $z = 0$ plane (except for the Y -function, where we take $z = 80$), while the right plots are for a plane containing the axis of symmetry.

variation, with Y approaching its extremum. Then there follows an intermediate region located inside the vortex, where X stays very close to zero, while the function Z is almost constant and close to its maximal value. (Typically, this region is on the order of 10^2 units of the fundamental length scale $1/M_\phi$.) There, the function X crosses the value zero on a circle of radius R at $z = 0$, with a small but non-zero first derivative, $\partial_r X(R, \pi/2) \neq 0$. Finally, there is a third region outside the vortex ring, where the fields approach their vacuum values. There, because of (3.54), the function Y has a slower decay than the functions X and Z . Also, both X and Z show large variations in a transition domain between the second and the third region, approaching afterwards very fast their asymptotic values.

The corresponding plots for the energy density $-T_t^t$ and the angular momentum density T_ϕ^t are shown in Figure 8. One can see that, as expected, the shape of T_ϕ^t copies the profile of the scalar function Z . However, the energy density distribution has some special features which single out vortons among the field theory solitons. For all studied configurations, the energy density has a local maximum at the origin²⁴, whose value decreases with n . Most of the vorton's energy is concentrated in a shell associated with a circular domain wall of cross-section r_0 . (The value of r_0 gives the transition between the second and third characteristic regions as defined above.) The center of this shell is located at $r = R, \theta = \pi/2$. Then, for the typical solutions in this work, the shape of the vorton energy density resembles a hollow tube (although there is always an almost constant nonzero value of T_t^t inside that tube). When the azimuthal winding number n increases, the position of this tube moves outwards. More relevant plots for typical solutions are given in Ref. [14] (see also the profiles in Figures 15, 16).

The vorton topology for a solution with $k = 1$ is illustrated by the diagrams in Figure 9. On the left picture we plot the lines of constant amplitude for the scalar ϕ (closed curves encircling the center of the vortex where ϕ vanishes) and phase (radial lines emanating from the center of the vortex) for a typical vorton

²⁴Note that, for spinning Q -balls, the energy density vanishes at $r = 0$. However, this is not the case for vortons, due to the nonzero contribution to T_t^t of the ϕ -field potential.

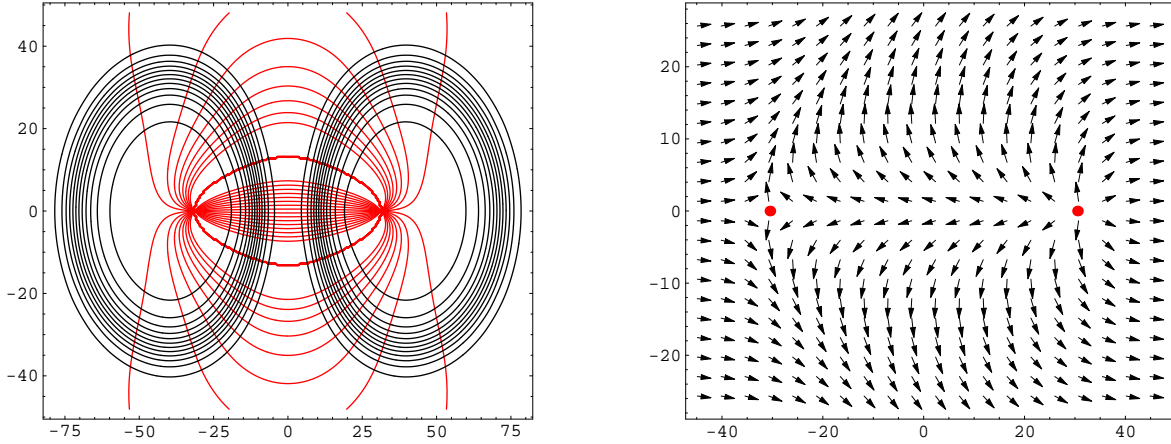


Figure 9. The behaviour of the field ϕ is displayed for a typical $k = 1$ vorton solution with $\beta_1 = 1$, $\beta_2 = 0.97$, $\beta_3 = 0.55$, $w = 0.13$ and $n = 2$. In the left panel we plot levels of constant amplitude $|\phi(x, 0, z)|$ (closed lines) and phase $\psi(x, 0, z)$ (radial lines). In the right panel, the horizontal and vertical length of each arrow is proportional to the real and imaginary part of ϕ (X and Y , respectively). The red points there indicate the position of the ring.

solution. The same picture is shown on the right panel in a different representation. There, the horizontal and vertical length of each arrow is proportional to the real and imaginary part of ϕ (X and Y , respectively). One can see, for instance, that the function Y takes significant values only in a region with a radius of about $50/M_\phi$, surrounding the vorton's core.

A systematic analysis of the parameter space of vorton solutions would be a very difficult task that we did not aim at here. Also, unfortunately, some regions of the parameter space are not accessible within our numerical approach. The solutions investigated so far cover a domain centred around the point²⁵ $\{\beta_1 = 1, \beta_2 = 0.95, \beta_3 = 0.5\}$, with maximal deviations of β_i around these values of about 7 percent. Also, all configurations reported here (including the gravitating solutions discussed in Section 4.2 below) represent thick vortons. Thus the radius of the vortex ring does not differ significantly from the thickness of the vortex. The constructions of thin vortons seems to require large values for the winding number n . However, we did not yet manage to find within our numerical approach solutions with $n > 6$ with high numerical accuracy.

We also mention that these vortons have been constructed by descending from solutions of the sigma model limit (2.11), where the constraint $X^2 + Z^2 + Y^2 = 1$ is satisfied. However, most of the solutions in this work exhibit large deviations from this value, with $|\phi|^2 + |\sigma|^2$ ranging typically from about 0.8 to about 1.1.

The picture we have found when attempting to vary the input parameters seems to be rather similar to the one found in the $k = 0$ case. (Although, for true vortons, the study of the limiting solutions is much more difficult.) In particular, the dependence of the solutions on the frequency looks qualitatively similar to the one exhibited in Figure 4. The Q -ball type behaviour is recovered. The solutions exist for a limited range of frequencies, and $M(Q)$ exhibits again two branches. (Plots illustrating this behaviour can be found in Ref. [14].)

Provided both $k = 0$ and $k = 1$ solutions exist for a given set of parameters, then the mass and angular momentum of the $k = 1$ solutions are found to be usually larger than those of the corresponding $k = 0$ configurations. (Note, that we could construct $k = 0$ ‘semitopological’ vortons for a much larger set of values of the potential parameters β_i than in the $k = 1$ case.)

An interesting feature of the $k = 1$ solutions which, to our knowledge, has not been reported so far in the literature is their nonuniqueness. This means that for the same input parameters (β_i, n, w) we have found two vorton solutions with different global charges. The situation is illustrated in Figure 10, where we plot a

²⁵The thin vorton solutions in [18] have been constructed for a choice of the parameters of the potential $\beta_1 = 1, \beta_2 = \beta_3 = 2/3$.

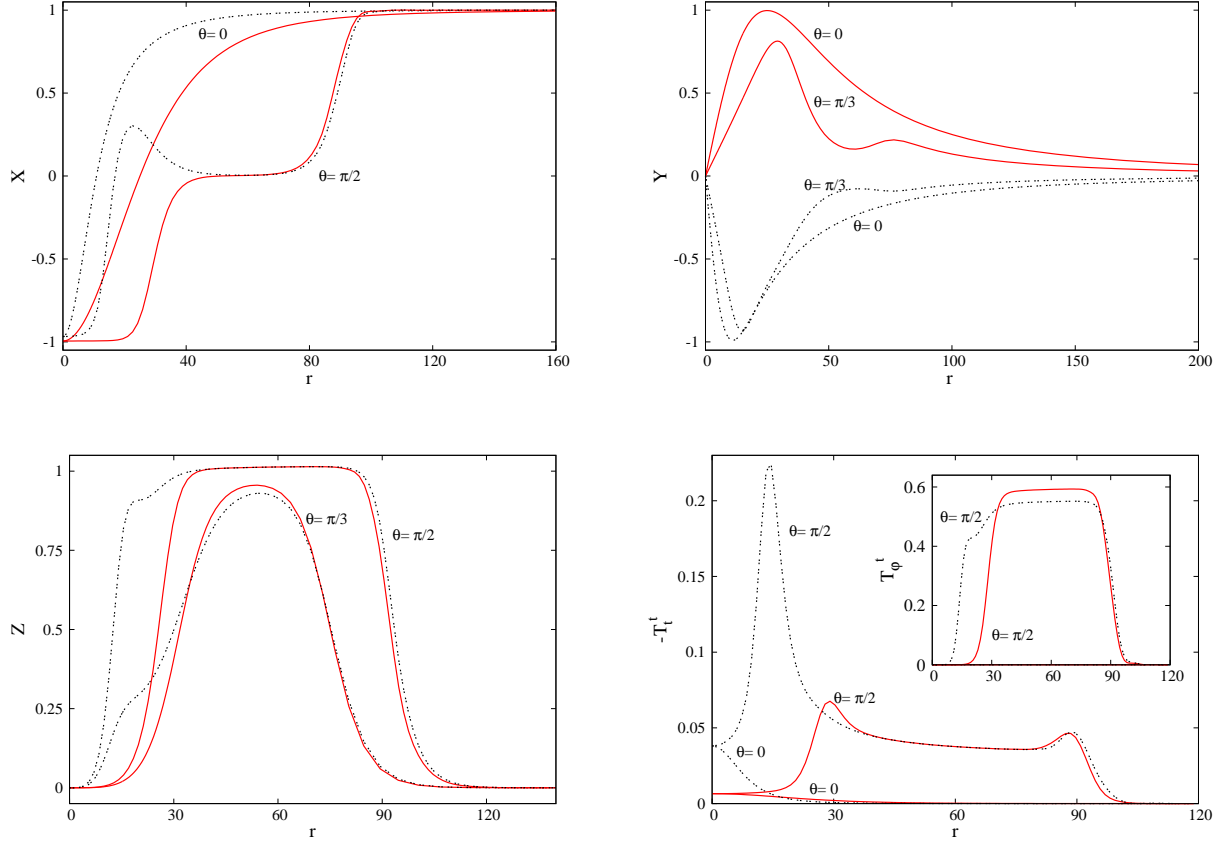


Figure 10. The profiles of the scalar functions $X(r, \theta)$, $Y(r, \theta)$, $Z(r, \theta)$ and of the energy density $-T_t^t$ are shown for two different $k = 1$ vorton solutions with the same input parameters: $\beta_1 = 1$, $\beta_2 = 0.97$, $\beta_3 = 0.54$, $w = 0.135$ and $n = 4$. The solution with dotted lines has higher mass and angular momentum and is an excitation of the fundamental solution, shown with solid lines.

fundamental solution, with lower mass (continuous line) together with the corresponding excited one (dotted line). The difference between the masses and charges of these two solutions increases with the winding number n . For the parameters in Figure 10 one finds *e.g.* $M^{(\text{fund.})}/M^{(\text{excit.})} \simeq 0.98$ for $n = 2$, while $M^{(\text{fund.})}/M^{(\text{excit.})} \simeq 0.9$ for $n = 5$. Interestingly, the solutions with higher mass have a smaller radius than the lower mass (and thus fundamental) configurations. Also, the excited configurations display a more complicated behaviour of the function X at $\theta = \pi/2$, exhibiting always an intermediate local extremum there. The profiles of the energy densities for the fundamental and excited solutions look also very different, see Figure 10. (Note also, that in Figures 7, 8, 9 we have displayed fundamental solutions; this holds also for all configurations reported in [14]).

These excited states are expected to be unstable. They are much more difficult to construct than the fundamental solutions²⁶. For the input parameters investigated so far, all fundamental solutions appear to possess excited configurations. However, the generic picture is likely to be more complicated, and other excited solutions may exist as well. For example, the nonuniqueness of solutions for the same input parameters and the same topological sector has been noticed in [44, 45] for the case of Yang-Mills-Higgs theory, with a Higgs field in the adjoint representation. As shown there, new branches of solutions appear at critical values of the strength of the Higgs self-coupling parameter λ .

²⁶The excited solutions have been found as limiting configurations of a secondary branch of gravitating solutions, see the discussion in Section 4.2.

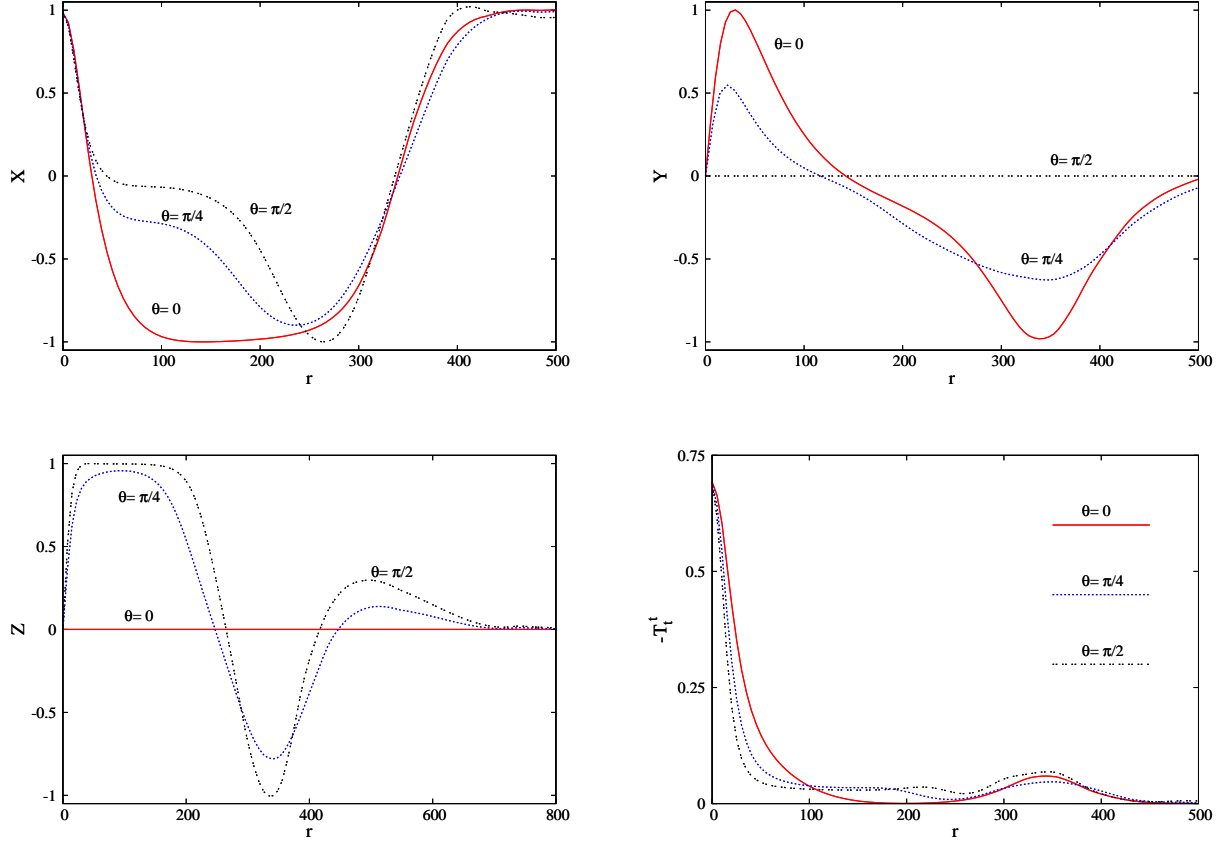


Figure 11. The profiles of the scalar functions $X(r, \theta)$, $Y(r, \theta)$, $Z(r, \theta)$ and of the energy density $-T_t^t$ are shown for a typical di-vorton with $\beta_1 = \beta_2 = 1$, $\beta_3 = 0.5$, $w = 0.023$, $n = 1$.

In this work we have only studied the dependence on the frequency of the excited solutions for fixed β_i, n . The results show that the picture found in [14] for the fundamental configurations holds also in this case.

Also, it is not clear to us how to interpret the nonuniqueness result in terms of the heuristic construction discussed in Section 3.1. This would imply the existence of excited vortex states for the same input data. (The corresponding ansatz is given by (3.51) with $k = 1$.) However, so far we could not construct such configurations.

3.4 Composite configurations. The di-vortons

As noted in the introduction, there is a striking analogy between the heuristic construction of a vorton (starting with a vortex) and that of a black ring (starting with a black string). However, in the gravity case, a variety of solutions describing composite configurations (*e.g.* a Saturn [46] and a di-ring [47]) have been constructed inspired by rather similar arguments. Thus it is reasonable to expect that the global Witten model (and, in general, any field theory model admitting vorton solutions) would also possess composite solutions—the analogs of $d = 5$ gravitating Saturn, di-ring and further multi-component objects.

In what follows we give some preliminary numerical evidence for the existence of a solution describing two concentric vortons, *i.e.* a di-vorton. In a heuristic construction, this configuration is found by taking finite pieces of two parallel vortices and bending them in the same plane, around a common center. Again, the resulting configuration would be supported against collapse by the centrifugal force.

The profile of a typical di-vorton solution is shown in Figure 11. There one can see that $|\phi|$ vanishes in the equatorial plane $\theta = \pi/2$, for two different values of r . These values correspond to the positions of

the two concentric rings. Also, the functions X, Y, Z show a much more complicated dependence on r and θ than in the single vorton case. One can see *e.g.* that, different from the single vorton case, the function X starts from a positive value at $r = 0$ (which is close to one, for all solutions we could construct), takes negative values for some range of r and approaches the *v.e.v.* $X = 1$ asymptotically. The mass and angular momentum of these solutions are much larger than the mass of two (usual) vortons with the same values of the input parameters. (Note also, that all di-vorton solutions we could construct so far correspond to configurations close to the sigma-model limit.) The angular momentum of the solutions is concentrated in two tori centred around the locations of the rings²⁷, while the mass density exhibits a local extremum at $r = 0$. The two radii of the di-vorton are also much larger than in the single vorton case.

The numerical accuracy was much lower in this case, which has prevented us from a systematic study of di-vortons. However, we expect them to share the basic properties of the usual vortons. In particular, they should exist for a limited range of frequencies.

4 Gravitating vortons

When α is increased from zero, while keeping $(\beta_i; n, w)$ fixed, a branch of rotating solutions emerges from the flat spacetime configurations. Since the dependence on α is different for $k = 0, 1$ solutions, we shall discuss them separately.

4.1 Gravitating $k = 0$ ‘semitopological’ vortons

Not entirely surprising, some properties of the gravitating $k = 0$ solutions are similar to those of the even-parity rotating boson stars in a model with a single complex scalar field [16].

The behaviour of a typical $k = 0$ solution is exhibited in Figure 12. These two-dimensional plots exhibit the small- r dependence for three angles $\theta = 0, \pi/4$ and $\pi/2$. (We recall that these solutions are symmetric *w.r.t.* an equatorial plane reflection.) One can notice, for example, that the functions f, l and m exhibit a strong angular dependence, with $l \neq m$ (except on the z -axis). Also, the metric functions are completely regular and the line element shows no sign of a horizon. However, the shape of the scalar functions X, Z is similar to that found for solutions in a flat spacetime background.

Considering the spatial structure of the solutions, we have found that the scalar fields X, Z typically give rise to a torus-like energy density, just as for the flat spacetime solutions. (This torus-like shape becomes apparent by considering surfaces of constant energy density.) Again, the maximum of the energy density of the solutions increases and shifts towards larger values of the coordinate $\rho = r \sin \theta$, when n (and thus the angular momentum) increases.

To demonstrate the effects of gravity, we exhibit in Figure 13 the mass and angular momentum of typical solutions as a function of frequency. Three different values of α are considered there, for the same parameters β_i of the potential and a winding number $n = 1$. Similar to the case of a flat spacetime background, the solutions exist for a limited range of frequencies, $w_{min} < w < w_{max}$, with w_{max} given by (3.55). However, as expected, the divergencies of the global charges at the limits of the w -interval which were found for $\alpha = 0$ (see Figure 6) are regularized by the effects of gravity. Moreover, for $\alpha \neq 0$, the solutions exhibit a complicated pattern after approaching w_{min} . There one observes an inspiralling behaviour of the $k = 0$ solutions, towards a limiting solution at the center of the spiral, for a frequency $w_{lim} > w_{min}$. (This behaviour could be studied more precisely for spherically symmetric solutions ($n = 0$), which we do not display here.) As a result, when the mass M is considered as a function of the scalar charge Q , we observe a cusp structure, as illustrated in Figure 13 (right). This is essentially the behaviour noticed in [16] for rotating boson stars. The branches starting from the maximal value of the frequency and ending at the maximal values of the mass are expected to be stable, in analogy to boson stars.

The dependence on the parameter α is shown in Figure 14. (A similar behaviour has been found for spherically symmetric solutions, $n = 0$.) One can see that the solutions exist for arbitrarily large values of

²⁷Different from the case of a Saturn [46] or of a di-ring [47] in $d = 5$ Einstein gravity, both components of a di-vorton carry an angular momentum density with the same sign, see the flat spacetime limit of the relation (2.31).

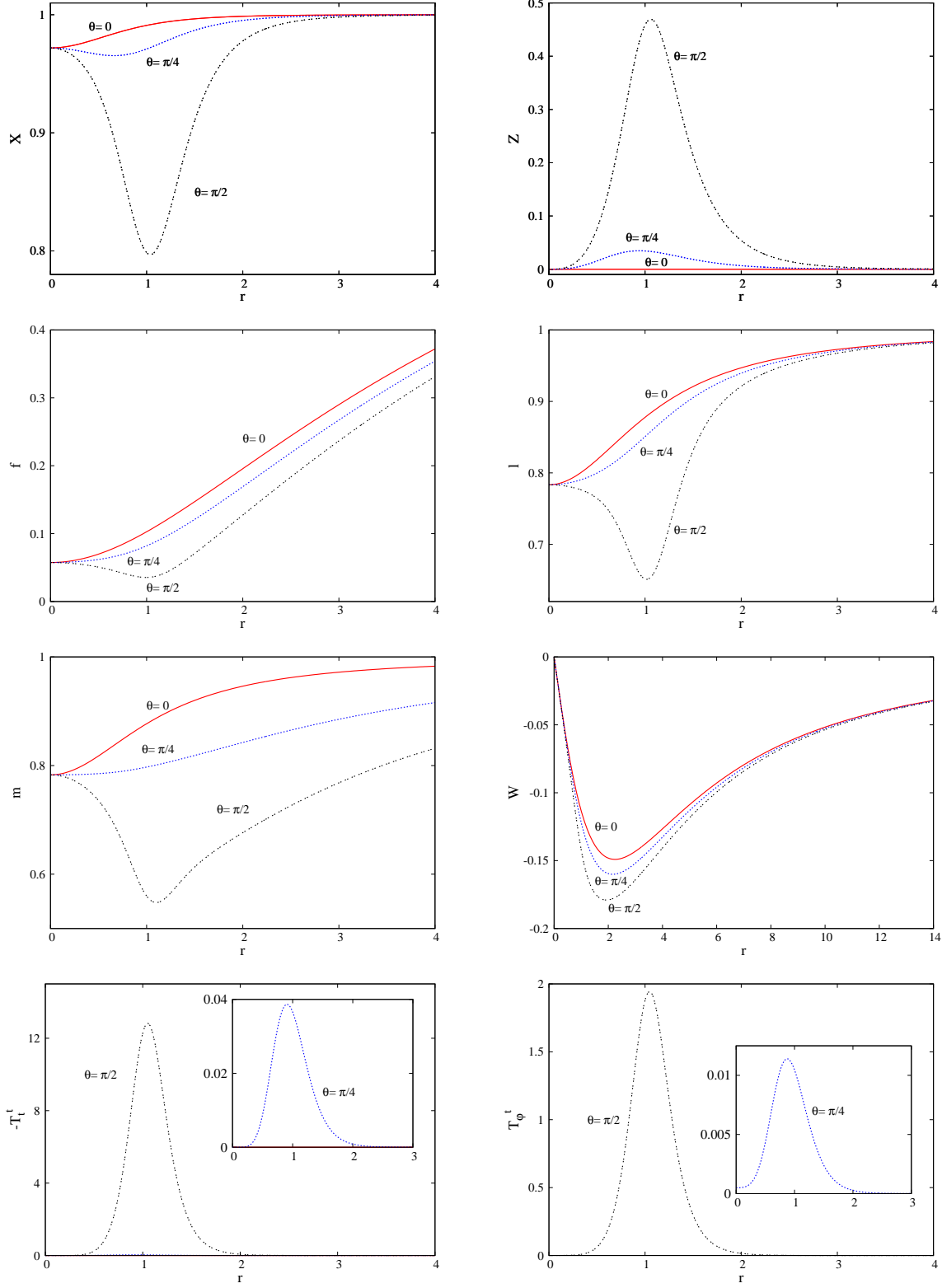


Figure 12. The functions $(X, Z; f, l, m, W)$ and the components T_t^t and T_ϕ^t of the energy-momentum tensor are shown for a $k = 0$ gravitating solution with $\beta_1 = 0.035$, $\beta_2 = 1$, $\beta_3 = 2.5$, $w = 0.79$, $n = 3$ and $\alpha = 1$.

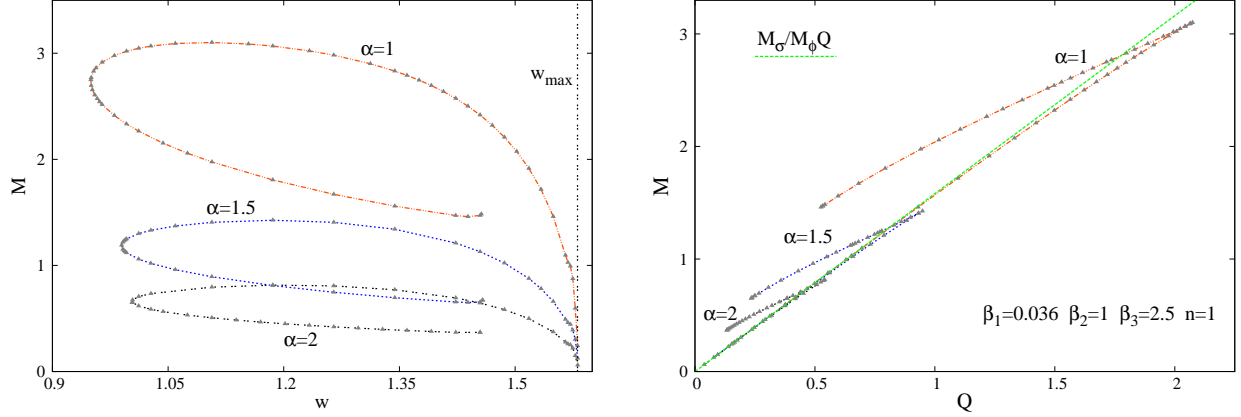


Figure 13. *Left:* The mass of gravitating $k = 0$ ‘semitopological’ vortons is shown as a function of the frequency for several values of the coupling constant α . The vertical line corresponds to the maximal value of the frequency as given by (3.55). Other input parameters of these configurations are $\beta_1 = 0.03$, $\beta_2 = 1$, $\beta_3 = 2.5$, $n = 1$. *Right:* The mass-charge diagram for the same solutions. Also we show the mass for Q free bosons, $M = M_\sigma/M_\phi Q$ in the units employed here.

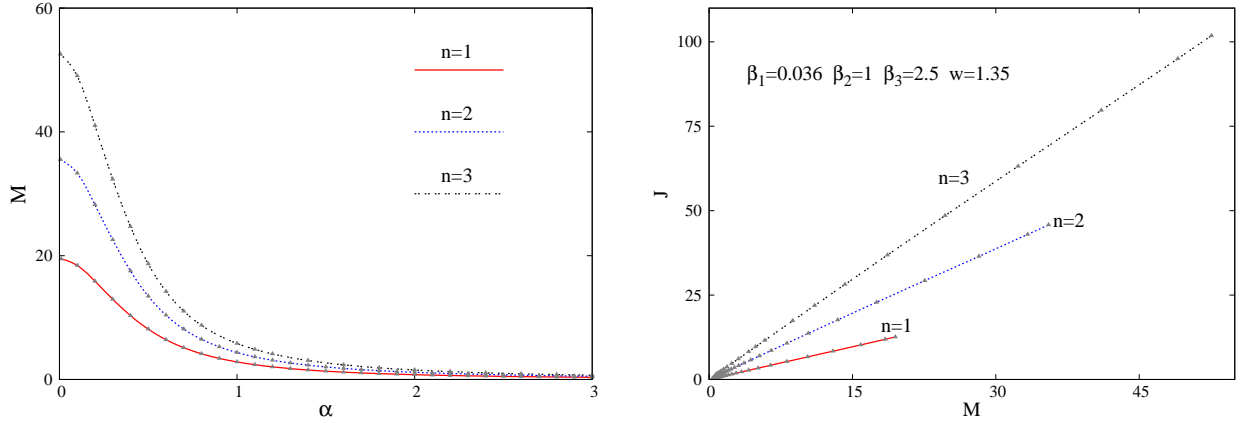


Figure 14. The mass and angular momentum are shown as functions of α for gravitating $k = 0$ ‘semitopological’ vortons.

α (*i.e.* an arbitrarily large *v.e.v.* of the scalar field ϕ).

This strongly contrasts with the picture found for other models featuring scalar fields with a symmetry breaking potential, *e.g.* monopoles or sphalerons, in which case a maximal value of α is found (see the review [21]). In the large α limit, the function Z vanishes, while the function X approaches a constant value everywhere, $X \rightarrow 1$, corresponding to the *v.e.v.* of the scalar field.

To understand this behaviour, we consider the scaled functions

$$\hat{X} = \frac{X-1}{\alpha}, \quad \text{and} \quad \hat{Z} = \frac{Z}{\alpha}, \quad (4.59)$$

Then, after making this replacement in the field equations and taking the limit $\alpha \rightarrow \infty$, the functions \hat{X}, \hat{Z}

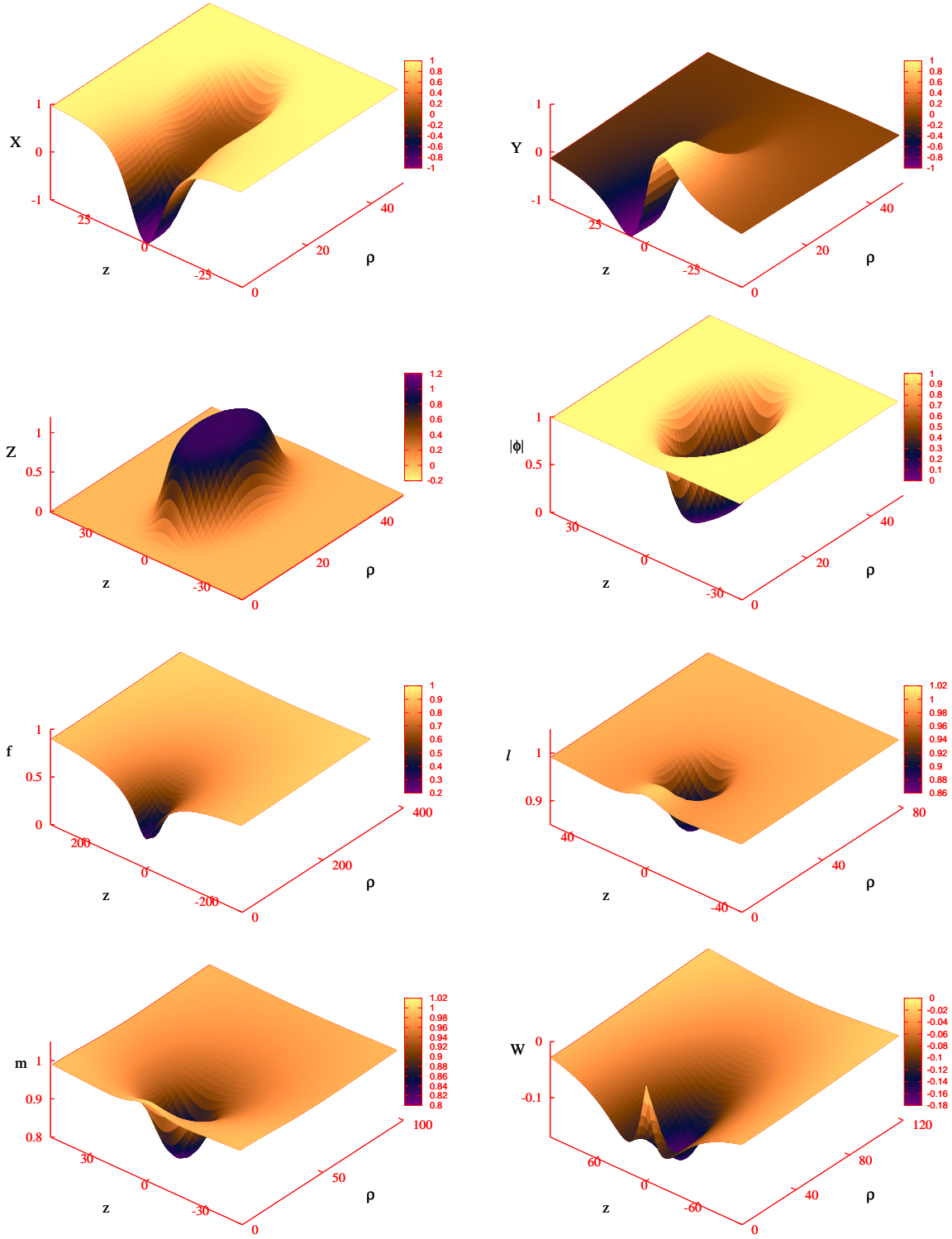


Figure 15. The scalar functions X , Y , Z , the amplitude $\sqrt{X^2 + Y^2}$ of the scalar field ϕ and the metric functions f, l, m, W are shown for a $k=1$ gravitating vorton solution with $\beta_1 = 1$, $\beta_2 = 0.97$, $\beta_3 = 0.54$, $w = 0.11$, $n = 3$ and $\alpha = 0.2$. The coordinates here are $\rho = r \sin \theta$ and $z = r \cos \theta$.

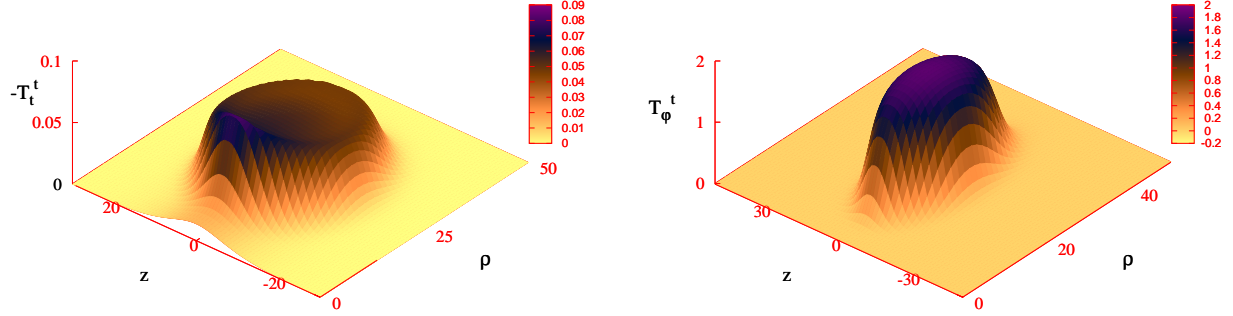


Figure 16. The energy density $-T_t^t$ and the angular momentum density T_φ^t are shown for the same solution as in Figure 15.

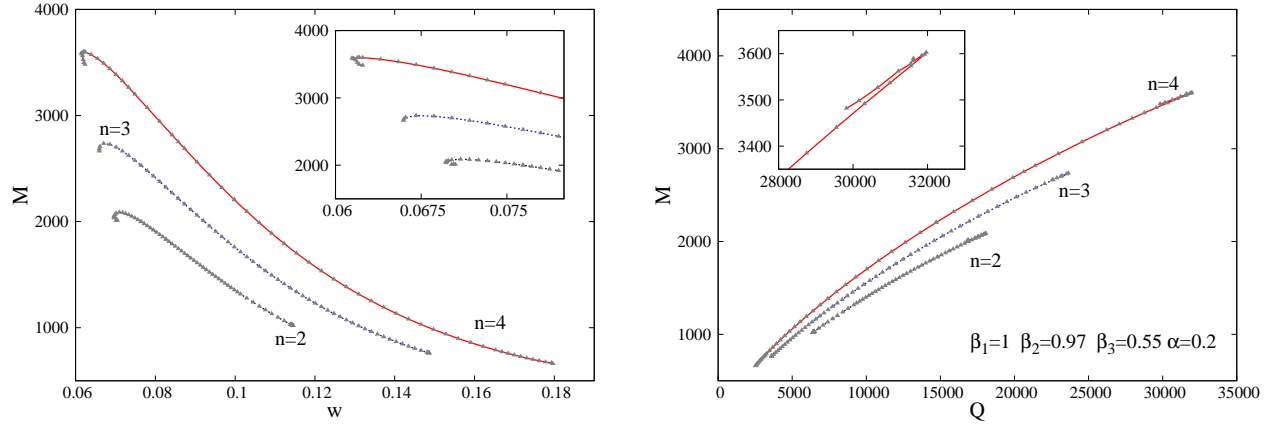


Figure 17. *Left:* The mass of gravitating $k = 1$ vortons is shown as a function of the frequency for several values of the winding number n . Other input parameters of these configurations are $\beta_1 = 1$, $\beta_2 = 1$, $\beta_3 = 0.54$ and $\alpha = 0.2$. *Right:* The mass-charge diagram for the same solutions.

decouple, the scaled matter fields being described by the Lagrangian

$$L_s = \partial_\mu \hat{X} \partial^\mu \hat{X} + \partial_\mu \hat{\sigma}^* \partial^\mu \hat{\sigma} + M_\sigma^2 |\hat{\sigma}|^2, \quad (4.60)$$

(with $\hat{\sigma} = \hat{Z} e^{i(n\varphi + wt)}$). It is clear that $\hat{X} = 0$ is the only physical solution, and we recover a boson star model for the complex scalar field $\hat{\sigma}$ possessing a quadratic potential. A similar behaviour has been found in [16] for gravitating Q -ball solutions with higher order terms in the potential: for large values of the coupling constant α , all higher order terms in the scalar field potential become irrelevant.

4.2 Gravitating $k = 1$ vortons

Again, these solutions smoothly emerge from configurations in a fixed Minkowski background. The backreaction is included by slowly increasing the value of α .

The 3D profiles of a typical solution are shown in Figure 15 as functions of the (scaled-)coordinates $\rho = r \sin \theta$ and $z = r \cos \theta$. One can notice the nontrivial behaviour of the metric functions, which strongly

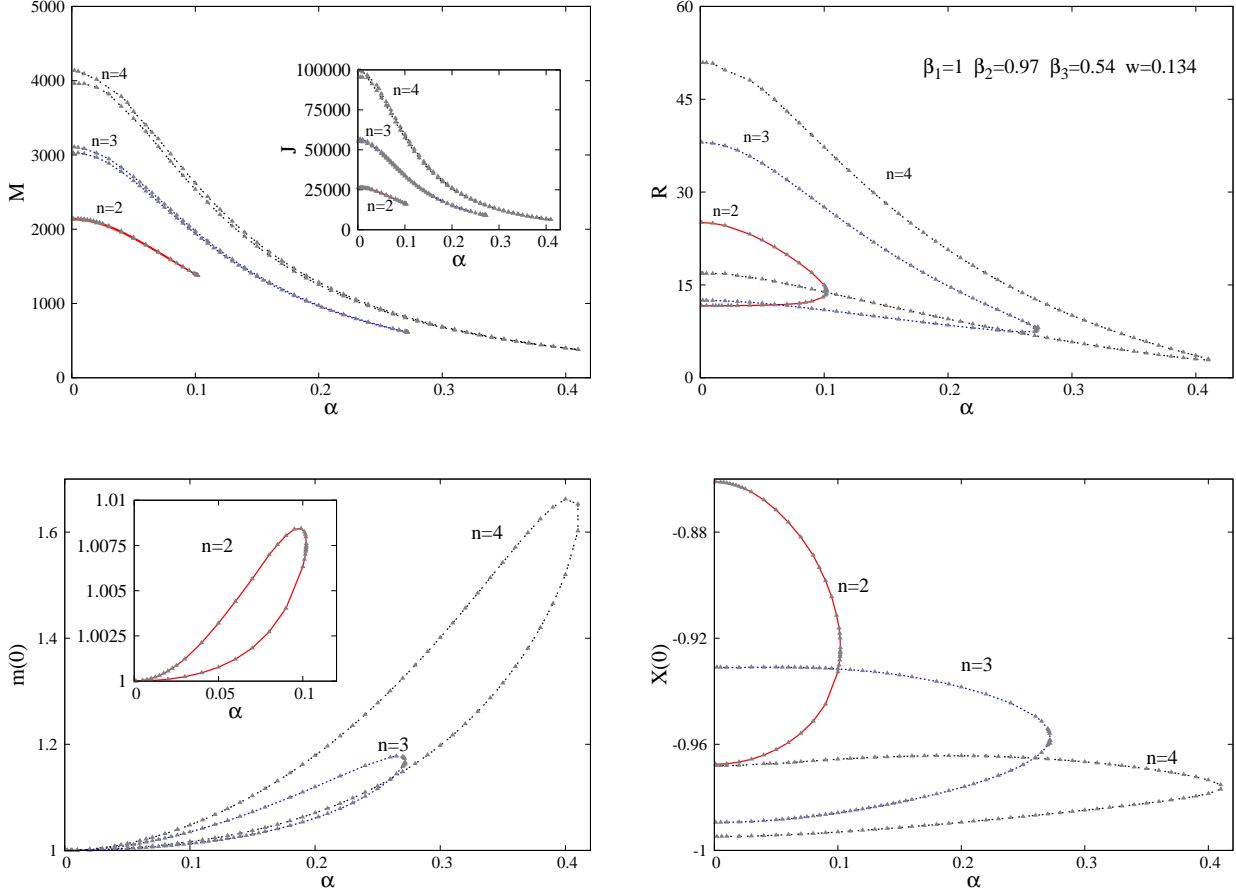


Figure 18. The mass M , radius of the ring R and the values at the origin of the metric function m and of the scalar function X are shown as functions of the parameter α for gravitating vorton solutions with $\beta_1 = 1$, $\beta_2 = 0.97$, $\beta_3 = 0.54$, $w = 0.13$ and several values of the winding number n . One can notice the existence of two branches of solutions connecting different flat spacetime ($\alpha = 0$) limiting configurations.

deviate from the flat spacetime values. The functions f, l and m approach their minimal value in the equatorial plane at the location of the ring where $X = 0$. For all solutions studied so far, we did not notice a special behaviour for the functions X, Y, Z in the gravitating case as compared to the flat spacetime limit.

The same holds for the distribution of the energy and angular momentum densities. In particular, as seen in Figure 16, the vorton energy density still resembles a hollow tube. (Note, that the local peak at $r = 0$ of the energy density is much smaller for this $n = 3$ solution than for the configuration with $n = 2$ exhibited in Figure 8.)

As expected, new effects occur when considering the vortons' dependence on the frequency. This is shown in Figure 17 for a typical family of gravitating solutions emerging from a flat spacetime fundamental configuration. One can see that some features found for $k = 0$ 'semitopological' solutions are likely to hold also in this case. For example, the range of w is bounded, both M and J approaching a maximum close to a minimal value of the frequency w_{min} . Furthermore, as for the $k = 0$ solutions, we notice the existence at w_{min} of a backbending towards larger values of w , leading apparently also to an inspiralling of the solutions towards a limiting configuration. Unfortunately, despite our efforts, numerical accuracy currently does not allow us to continue the construction of the (expected) spiral in a reliable way.

This holds also for the issue of a maximal frequency, in which case we could not construct the counterparts of the curves in Figure 13, with a fast decreasing mass and charge. The situation here is puzzling, since, for all considered sets of input parameters ($\beta_i; n; \alpha$), we could not construct $k = 1$ gravitating vortons with

frequencies below a critical value w_c . As $w \rightarrow w_c$, the solver diverges, or, more often, provides a solution of the problem with $Y = 0$. At the same time, we do not notice any special features of the $k = 1$ configurations close to w_c ; in particular the metric functions do not exhibit any pathological behaviour. Interestingly, the $k = 0$ configuration which is found in this way possesses almost the same mass and angular momentum as the $k = 1$ vorton solution with $w \rightarrow w_c$ (although other relevant parameters (*e.g.* the value of the metric function f at the origin) are different). Then one may speculate that the $k = 1$ branch would continue for $w > w_c$ with a branch of $k = 0$ configurations towards w_{max} given by (3.55), where the vacuum state is approached²⁸. However, due to limitations, resulting from our numerical treatment of the problem, we could not clarify this point.

A distinct feature of the $k = 1$ gravitating vortons is their dependence on α . The emerging picture which results from the study of several different sets of solutions can be summarized as follows²⁹: given a fundamental flat spacetime configuration with a set of input parameters $(\beta_i; n, w)$, the curved spacetime configurations are found by increasing the parameter α . The emerging branch of solutions exists up to a maximal value of α (which depends on the input parameters).

As $\alpha \rightarrow \alpha_{max}$ all relevant quantities stay finite. (In particular, we do not see any sign for the emergence of an event horizon.) At α_{max} a second branch of solutions is found, extending backwards in α . As $\alpha \rightarrow 0$, this branch approaches the excited flat spacetime vorton discussed in Section 3.3. These features are illustrated in Figure 18. (We mention that the ring radius R , the absolute value of the scalar function X and the value of the metric function m at the origin are smaller for solutions on the excited branch.)

The fact that there is an upper bound on α for $k = 1$ solutions can be understood as follows. A similar scaling to (4.59) (this time also with $\hat{Y} = Y/\alpha$) shows that the limit $\alpha \rightarrow \infty$ would imply necessarily $\hat{X} \equiv 0$ (thus $X \equiv 1$), $\hat{Y} \equiv 0$. However, these values cannot be continuously approached, since $|\phi|$ should always vanish on a circle in the equatorial plane. In other words, since $k = 0$ and $k = 1$ correspond to different ‘topological’ sectors of the theory, no continuous transition between them is possible³⁰.

As a result, the solutions exhibit instead a maximal value of the parameter α , with a backbending towards a second $\alpha = 0$ solution in a flat spacetime background³¹.

Thus we have reached the important conclusion³² that the effects of gravity impose an upper bound on the *v.e.v.* η_ϕ of the scalar ϕ for solutions to exist. This upper bound depends on the parameters of the model, with a general expression

$$\alpha^2 = \frac{16\pi}{\lambda_\phi} \left(\frac{M_\phi}{M_{Pl}} \right)^2 < c, \quad (4.61)$$

with c a parameter of order one, whose precise value depends on the other input data.

Rotating objects in general relativity may possess ergoregions. However, unlike the case of black holes, the ergoregions of regular objects like those in this work would signal the presence of an instability [49].

Within the metric ansatz (2.21), the ergosurface is defined by the condition

$$g_{tt} = -f + \frac{l}{f} W^2 \sin^2 \theta = 0. \quad (4.62)$$

²⁸Note also that, since $|\phi|$ vanishes on a circle in the equatorial plane, the vortons cannot approach in a continuous way the vacuum state with $X \equiv 1, Y \equiv 0$.

²⁹However, we do not exclude that a different picture may exist for other sets of parameters, not considered in this work.

³⁰It may be interesting to note, that we could not construct solutions in which the function Y takes very small values and can be considered as a perturbation around a configuration featuring only the X, Z functions. Related to that, for all solutions with $Y \neq 0$, the function X possesses a node in the equatorial plane.

³¹We would like to mention that the physical meaning of the second limiting solution is not obvious *a priori*. Since $\alpha \rightarrow 0$ can be reached also when taking $\eta_\phi \rightarrow 0$ (see (2.47)), the limiting solution might represent a scaled boson star in a model featuring only the scalar field σ coupled to gravity. However, as seen in Figure 18, this is not the case, at least for the solutions in this work.

³²One should also mention that, different from most of the other gravitating solutions with a scalar field featuring a *v.e.v.*, we did not find any indication for the existence of black hole solutions. (Typically, they emerge from the globally regular configurations for a critical value of α [21].) This property should be attributed to the Q-ball features of the vortons induced by the field σ . In fact, for the simplest case $k = 0, n = 0$, one can prove the absence of black hole solutions following the arguments in [48]. A similar result may hold also in the spinning case. Note, that this is not obvious, since the approach used in [48] cannot be easily generalized to the rotating case. In fact, spinning black holes with complex scalar fields possessing a harmonic time dependence have been constructed recently in [32] for a five dimensional anti-de Sitter spacetime background. (They require a fine tuning between the frequency of the field and the event horizon velocity.)

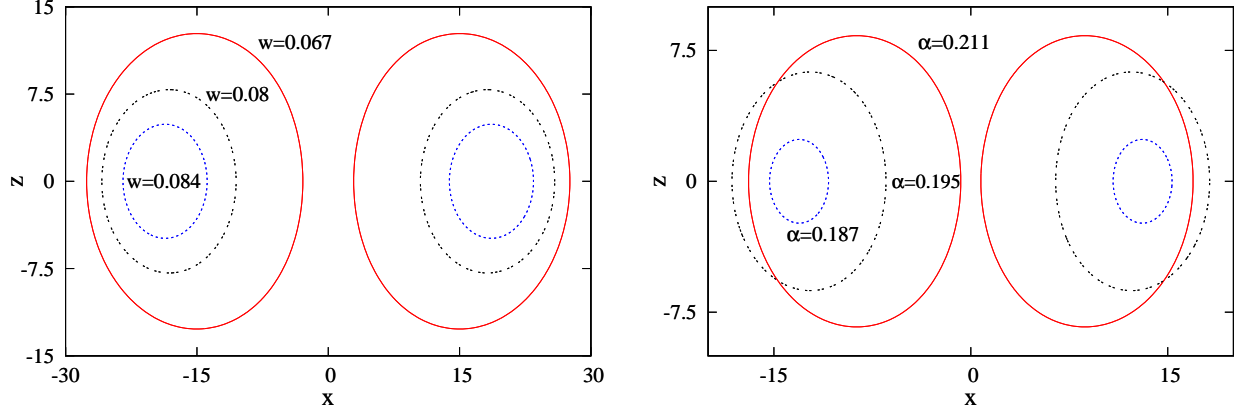


Figure 19. The location and shape of the vortons' ergoregion is exhibited for solutions with three different frequencies (left) and three different values of α (right). The parameters of the potential are $\beta_1 = 0.14$, $\beta_2 = 0.974$, $\beta_3 = 0.54$ while $\alpha = 0.2$, $n = 3$ (left) and $w = 0.07$, $n = 2$ (right).

Then the ergoregion resides inside this ergosurface. Examining the condition (4.62), we find that this is not satisfied for most of the gravitating vorton solutions. For example, when varying the frequency, the ergoregion typically occurs for a set of solutions close to the backbending point at w_{min} , in particular, for secondary branch configurations. The solutions with large enough frequencies (in particular those close enough to w_{max}) have $g_{tt} < 0$. (This is again similar to the situation encountered for boson stars [16].)

When studying instead the influence of the parameter α , we find that an ergoregion may occur for a set of solutions close to α_{max} (and with values of w not too far from w_{min}). That is, for the parameter choice in this work, the solutions with small values of α (which are expected to be relevant in a realistic context) do not exhibit an ergoregion. Some results displaying these features are shown in Figure 19. One can see that the vortons' ergoregions also possess a toroidal shape, whose size and location depend on the input parameters. Without entering into details, we mention the existence of similar results for $k = 0$ 'semitopological' vortons, where some of these solutions also possess an ergoregion.

We close this part by remarking that the di-vortons should also possess gravitating generalizations. However, due to the severe numerical difficulties, we could construct such solutions for very small values of α only. Their systematic study might possibly require a different numerical approach.

5 Discussion and conclusions

More than 20 years after vortons have been first proposed, they continue to provide an interesting field of research. Posing a severe numerical challenge, the systematic quantitative study of such configurations has started only recently [14, 18], within the global version of Witten's $U(1) \times U(1)$ theory.

The first purpose of this work was to give an overview of the properties of vortons in a flat spacetime background. The heuristic construction of these objects as reviewed in Section 3.1 suggests to view the usual vortons as the second member ($k = 1$) of a family of solutions indexed by the number of nodes k of the vortex field ϕ . Then the case $k = 0$ would correspond to 'semitopological' vortons. These solutions could be studied to a greater extent and seem to exhibit most of the basic properties of the usual vortons ($k = 1$). A new result reported in Section 3.3 is the nonuniqueness of the vortons for the same input parameters. There we have given numerical evidence for the existence of excited solutions, which play an important role when including the gravity effects. Another new type of configuration describing two concentric rings, the di-vorton, has been reported in Section 3.4. Here we remark that one expects that Witten's model possesses a variety of other composite configurations. For example, it would be interesting to find a solution describing a 'Saturn' *i.e.* a configuration with a central concentration of the energy density surrounded by a ring (this would correspond to different zeros of the scalar field ϕ).

Another aim of this work was to present a first discussion of how gravity affects the properties of $k = 0$ ‘semitopological’ vortons and $k = 1$ ‘true’ vortons. Our results can be summarized as follows. First, we have shown that, when varying the frequency, gravity imposes an upper bound on the mass and angular momentum of these objects. The coupling to gravity gives rise to a spiral-like frequency dependence of the mass and charge. Second, we have noticed a different behaviour of the $k = 0$ and $k = 1$ solutions as functions of the parameter α , describing the coupling to gravity. The $k = 0$ solutions are essentially ‘dressed’ Q-balls in a more complicated version of the FLS model [22]. (This holds also in the flat spacetime limit.) Different from true vortons, the limit $\alpha \rightarrow \infty$ is allowed in this case. For $k = 1$, one finds instead two branches of solutions joining at a maximal value of α . Finally, we have noticed that, similar to the boson star case, vortons may possess an ergoregion, with the associated instability. Here one should say that a systematic study of the dependence of the properties of the vortons on the various input parameters is still missing and continues to present a numerical challenge.

As avenues for future research, perhaps the most compelling task would be the study of vortons in models including gauge fields as well. The simplest case here would be again the local version of Witten’s $U(1) \times U(1)$ theory. The corresponding gauged vortons could be constructed by using a similar approach to that described in this work and will be reported elsewhere.

However, vortons should also exist in other more complex models, *e.g.* possessing non-Abelian fields apart from scalars. An interesting question to ask in this context is the possible existence of ‘springs’ [51], *i.e.* vortex loops stabilized by magnetic fields instead of rotation³³. While ‘spring’ solutions are unlikely to exist in Witten’s $U(1) \times U(1)$ theory, such configurations have been found in other models featuring non-Abelian fields, see *e.g.* [52, 53].

Then it would be interesting to reconsider some of the known toroidal solitons based on the heuristic construction of a vorton/‘spring’ starting with pieces of strings. For example, vortex ring solutions are known to exist in the Yang-Mills-Higgs model with the Higgs field in the adjoint representation [52]. However, these configurations seem to correspond³⁴ to loops made of Yang-Mills-Higgs vortices discussed in [54]. Finally, the possible existence of vortons and ‘springs’ in the electroweak sector of the Standard Model is perhaps the most exciting open problem (see [53, 55, 56, 57] for some work in this direction).

Acknowledgements.— E. R. would like to thank M. S. Volkov for introducing him to the subject of vortons and for fruitful collaboration on this topic. We also thank J. Garaud and M. S. Volkov for sending us their unpublished results on global vortons. We would like to thank B. Kleihaus and T. Tchrakian for discussions and remarks during various stages of this work. We gratefully acknowledge support by the DFG, in particular, also within the DFG Research Training Group 1620 “Models of Gravity”.

A System of differential equations

The metric functions f, l, m and W which enter the Ansatz (2.21) satisfy the following set of coupled non-linear partial differential equations:

$$\begin{aligned} \nabla^2 f - \frac{1}{f}(\nabla f)^2 + \frac{1}{2l}(\nabla f) \cdot (\nabla l) - \frac{l}{f}r^2 \sin^2 \theta (\nabla(\frac{W}{r}))^2 \\ + 16\pi Gm \left(-\frac{2(w + n\frac{W}{r})^2 Z^2}{f} + U(X, Y, Z) \right) = 0, \end{aligned} \quad (\text{A.1})$$

³³Note, that the static dipole black rings can be balanced by immersing them in a background magnetic field [50].

³⁴We thank F. Navarro-Lérida and T. Tchrakian for discussions on that and for sharing with us their unpublished results.

(A.2)

$$\nabla^2 l - \frac{1}{2l}(\nabla l)^2 + \frac{\partial_r l}{r} + \frac{\cot \theta}{r^2} \partial_\theta l + 32\pi G m \left(\frac{n^2 Z^2}{r^2 \sin^2 \theta} - (w + \frac{nW}{r})^2 \frac{l Z^2}{f^2} + \frac{l}{f} U(X, Y, Z) \right) = 0, \quad (\text{A.3})$$

$$\nabla^2 m + \frac{m}{2f^2}(\nabla f)^2 - \frac{1}{m}(\nabla m)^2 - \frac{3lm}{2f^2} r^2 \sin^2 \theta (\nabla(\frac{W}{r}))^2 - \frac{\partial_r m}{r} - \frac{\cot \theta}{r^2} \partial_\theta m \quad (\text{A.4})$$

$$+ 16\pi G m \left((\nabla X)^2 + (\nabla Y)^2 + (\nabla Z)^2 - (w + \frac{nW}{r})^2 \frac{m}{f^2} Z^2 - \frac{m}{l} \frac{n^2 Z^2}{r^2 \sin^2 \theta} + \frac{m}{f} U(X, Y, Z) \right) = 0,$$

$$\nabla^2 W - \frac{2}{f}(\nabla f) \cdot (\nabla W) + \frac{3}{2l}(\nabla l) \cdot (\nabla W) + \frac{2}{r^2} \left(\partial_r W + \frac{\cot \theta}{r} \partial_\theta W - \frac{W}{r} \right) \quad (\text{A.5})$$

$$- 32\pi G \frac{m}{l} \frac{n Z^2}{r^2 \sin^2 \theta} (w + \frac{nW}{r}) = 0.$$

They are equivalent to the following combinations of the Einstein equations: $E_t^t - E_r^r - E_\theta^\theta - E_\varphi^\varphi + \frac{2W}{r} E_\varphi^t = 0$ (for (A.1)), $E_r^r + E_\theta^\theta = 0$ (for (A.3)), $E_\varphi^\varphi - \frac{2W}{r} E_\varphi^t = 0$ (for (A.4)), and $E_\varphi^t = 0$ (for (A.5)), multiplied with suitable factors (*e.g.* $-m$ for (A.1)).

The equations for the scalar functions result directly from (2.9) and read:

$$\nabla^2 X + \frac{1}{2l}(\nabla l) \cdot (\nabla X) + \frac{m}{f} X \left(\frac{1}{2} \lambda_\phi (\eta_\phi^2 - X^2 - Y^2) - \gamma Z^2 \right) = 0,$$

$$\nabla^2 Y + \frac{1}{2l}(\nabla l) \cdot (\nabla Y) + \frac{m}{f} Y \left(\frac{1}{2} \lambda_\phi (\eta_\phi^2 - X^2 - Y^2) - \gamma Z^2 \right) = 0, \quad (\text{A.6})$$

$$\nabla^2 Z + \frac{1}{2l}(\nabla l) \cdot (\nabla Z) + \frac{m}{f} Z \left(\frac{1}{2} \lambda_\sigma (\eta_\sigma^2 - Z^2) - \gamma (X^2 + Y^2) - \frac{n^2}{r^2 \sin^2 \theta} \frac{f}{l} + \frac{(w + \frac{nW}{r})^2}{f} \right) = 0.$$

In the above relations we have defined

$$\nabla^2 A = \frac{1}{r^2} \frac{\partial}{\partial r} (r^2 \frac{\partial A}{\partial r}) + \frac{1}{r^2 \sin \theta} \frac{\partial}{\partial \theta} (\sin \theta \frac{\partial A}{\partial \theta}), \quad (\text{A.7})$$

$$(\nabla A) \cdot (\nabla B) = \frac{\partial A}{\partial r} \frac{\partial B}{\partial r} + \frac{1}{r^2} \frac{\partial A}{\partial \theta} \frac{\partial B}{\partial \theta}.$$

Also, $U(X, Y, Z)$ is the potential of the scalar fields, which results directly from (2.2) after substituting the scalar field ansatz (2.22)

$$U(X, Y, Z) = \frac{1}{4} \lambda_\phi (X^2 + Y^2 - \eta_\phi^2)^2 + \frac{1}{4} \lambda_\sigma Z^2 (Z^2 - 2\eta_\sigma^2) + \gamma (X^2 + Y^2) Z^2. \quad (\text{A.8})$$

These equations are supplemented with the following constraints

$$\frac{1}{l} \left(\partial_r^2 l - \frac{1}{r^2} \partial_\theta^2 l \right) - \frac{1}{lm} \left(\partial_r l \partial_r m - \frac{1}{r^2} \partial_\theta l \partial_\theta m \right) - \frac{1}{2l^2} \left((\partial_r l)^2 - \frac{1}{r^2} (\partial_\theta l)^2 \right) + \frac{1}{f^2} \left((\partial_r f)^2 - \frac{1}{r^2} (\partial_\theta f)^2 \right) \quad (\text{A.9})$$

$$- \frac{l \sin^2 \theta}{f^2} \left((\partial_r W)^2 - \frac{1}{r^2} (\partial_\theta W)^2 \right) + \frac{1}{rl} \left(\partial_r l - \frac{2 \cot \theta}{r} \partial_\theta l \right) - \frac{2}{rm} \left(\partial_r m - \frac{\cot \theta}{r} \partial_\theta m \right) + \frac{W l \sin^2 \theta}{f^2 r^2} (-W + 2r \partial_r W)$$

$$+ 32\pi G \left((\partial_r X)^2 + (\partial_r Y)^2 + (\partial_r Z)^2 - \frac{1}{r^2} ((\partial_\theta X)^2 + (\partial_\theta Y)^2 + (\partial_\theta Z)^2) \right) = 0,$$

$$\frac{1}{l} \partial_r \partial_\theta l + \frac{\partial_r f \partial_\theta f}{f^2} - \frac{\partial_r l \partial_\theta l}{2l^2} - \frac{l \sin^2 \theta}{f^2} \partial_r W \partial_\theta W - \frac{1}{2lm} (\partial_r m \partial_\theta l + \partial_r l \partial_\theta m) - \cot \theta \frac{\partial_r m}{m} - \frac{\partial_\theta m}{rm} \quad (\text{A.10})$$

$$+ \cot \theta \frac{\partial_r l}{l} + \frac{W l \sin^2 \theta}{r f^2} \partial_\theta W + 32\pi G (\partial_r X \partial_\theta X + \partial_r Y \partial_\theta Y + \partial_r Z \partial_\theta Z) = 0,$$

which result from the Einstein equations $E_r^r - E_\theta^\theta = 0$ for (A.9), and $E_r^\theta = 0$ for (A.10)).

B The nonvanishing components of the energy momentum tensor

The nonvanishing components of the energy-momentum tensor of gravitating vortons are found by substituting the ansatz (2.22) in the general expression (2.7) and read

$$\begin{aligned}
T_r^r &= (w + \frac{nW}{r})^2 \frac{Z^2}{f} - U(X, Y, Z) - \frac{1}{r^2 \sin^2 \theta} \frac{n^2 f}{l} Z^2 \\
&\quad + \frac{f}{m} \left[(\partial_r X)^2 + (\partial_r Y)^2 + (\partial_r Z)^2 - \frac{1}{r^2} ((\partial_\theta X)^2 + (\partial_\theta Y)^2 + (\partial_\theta Z)^2) \right], \\
T_r^\theta &= \frac{2f}{r^2 m} (\partial_r X \partial_\theta X + \partial_r Y \partial_\theta Y + \partial_r Z \partial_\theta Z), \\
T_\theta^\theta &= (w + \frac{nW}{r})^2 \frac{Z^2}{f} - U(X, Y, Z) - \frac{1}{r^2 \sin^2 \theta} \frac{n^2 f}{l} Z^2 \\
&\quad - \frac{f}{m} \left[(\partial_r X)^2 + (\partial_r Y)^2 + (\partial_r Z)^2 - \frac{1}{r^2} ((\partial_\theta X)^2 + (\partial_\theta Y)^2 + (\partial_\theta Z)^2) \right], \\
T_\varphi^\varphi &= (w^2 - \frac{n^2 W^2}{r^2}) \frac{Z^2}{f} - U(X, Y, Z) + \frac{1}{r^2 \sin^2 \theta} \frac{n^2 f}{l} Z^2 - \frac{f}{m} ((\nabla X)^2 + (\nabla Y)^2 + (\nabla Z)^2),
\end{aligned} \tag{B.1}$$

and finally, the most important components are

$$\begin{aligned}
-T_t^t &= \frac{f}{m} ((\nabla X)^2 + (\nabla Y)^2 + (\nabla Z)^2) + U(X, Y, Z) + \frac{1}{r^2 \sin^2 \theta} \frac{n^2 f}{l} Z^2 + (w^2 - \frac{n^2 W^2}{r^2}) \frac{Z^2}{f}, \\
T_\varphi^t &= 2n(w + \frac{nW}{r}) \frac{Z^2}{f},
\end{aligned} \tag{B.2}$$

corresponding to the energy density and the angular momentum density, respectively.

C Spherically symmetric solutions

These solutions occur as a limiting case of the general configurations. Their line element is found from (2.21) for $l = m$ and $W = 0$, and reads

$$ds^2 = \frac{m}{f} (dr^2 + r^2(d\theta^2 + \sin^2 \theta d\varphi^2)) - f dt^2, \tag{C.1}$$

the metric functions f and m depending only on the radial coordinate r . The scalar field ansatz results from (2.22) for $n = 0$ and reads

$$\phi = X(r), \quad \sigma = Z(r)e^{i\omega t}. \tag{C.2}$$

The equations greatly simplify in this case. From (A.6), (A.1), (A.4) one finds

$$\begin{aligned}
X'' + (\frac{m'}{2m} + \frac{2}{r})X' - \gamma \frac{m}{f} X Z^2 + \frac{\lambda_\phi}{2} \frac{m}{f} X (\eta_\phi^2 - X^2) &= 0, \\
Z'' + (\frac{m'}{2m} + \frac{2}{r})Z' + \frac{w^2 m}{f^2} Z - \gamma \frac{m}{f} X^2 Z + \frac{\lambda_\sigma}{2} \frac{m}{f} Z (\eta_\sigma^2 - Z^2) &= 0,
\end{aligned} \tag{C.3}$$

for the scalar fields, and

$$\begin{aligned}
f'' + (\frac{m'}{2m} + \frac{2}{r} - \frac{f'}{f})f' + 16\pi Gm \left(-\frac{2w^2 Z^2}{f} + U(X, Z) \right) &= 0, \\
m'' + \frac{m'}{r} - \frac{m'^2}{m} + \frac{m f'^2}{2f^2} + 16\pi Gm \left(X'^2 + Z'^2 - \frac{w^2 m Z^2}{f^2} + \frac{m}{f} U(X, Z) \right) &= 0,
\end{aligned} \tag{C.4}$$

for the metric functions (with $U(X, Z)$ given by (A.8) with $Y = 0$), together with the constraint (which results from (A.9))

$$\frac{m''}{m} + \frac{f'^2}{f^2} - \frac{m'}{rm} - \frac{3m'^2}{2m^2} + 32\pi G(X'^2 + Z'^2) = 0. \quad (\text{C.5})$$

The approximate form of the solutions as $r \rightarrow 0$ reads (note that Z does not vanish there)

$$f(r) = f_0 + f_2 r^2 + O(r^4), \quad m(r) = m_0 + m_2 r^2 + O(r^4), \quad (\text{C.6})$$

$$X(r) = x_0 + x_2 r^2 + O(r^4), \quad Z(r) = z_0 + z_2 r^2 + O(r^4). \quad (\text{C.7})$$

All coefficients in this expansion are fixed by the parameters f_0 , m_0 , x_0 and z_0 (one finds *e.g.* $x_2 = \frac{m_0 x_0}{6f_0} \left(\frac{\lambda_\phi}{2} (x_0^2 - \eta_\phi^2) + \gamma z_0^2 \right)$ and $z_2 = \frac{m_0 z_0}{6f_0^2} (-w^2 + f_0(\gamma x_0^2 - (\frac{\lambda_\sigma}{2}(z_0^2 - \eta_\sigma^2)))$). The large- r expression of the scalar functions X, Z results from (3.54) by taking $A = 0$. The leading order terms in the corresponding expansion of the metric function are

$$f(r) = 1 + \frac{f_1}{r} + \frac{f_1^2}{2r^2} + \dots, \quad m(r) = 1 - \frac{f_1^2}{8r^2} + \dots, \quad (\text{C.8})$$

with f_1 a parameter fixing the ADM mass of the solutions.

Some basic properties of these configurations are rather similar to those found for spinning $k = 0$ solutions. In particular, we have found the same qualitative dependence on the parameters w , α as in that case.

References

- [1] R. L. Davis and E. P. S. Shellard, Phys. Lett. B **209** (1988) 485.
- [2] R. L. Davis, Phys. Rev. D **38** (1988) 3722.
- [3] R. L. Davis and E. P. S. Shellard, Nucl. Phys. B **323** (1989) 209.
- [4] E. Witten, Nucl. Phys. B **249** (1985) 557.
- [5] R. H. Brandenberger, B. Carter, A. -C. Davis and M. Trodden, Phys. Rev. D **54** (1996) 6059 [hep-ph/9605382].
- [6] K. B. W. Buckley, M. A. Metlitski and A. R. Zhitnitsky, Phys. Rev. D **68** (2003) 105006 [hep-ph/0212074].
- [7] R. A. Battye, N. R. Cooper and P. M. Sutcliffe, Phys. Rev. Lett. **88** (2002) 080401 [cond-mat/0109448].
- [8] R. Emparan and H. S. Reall, Phys. Rev. Lett. **88** (2002) 101101 [hep-th/0110260].
- [9] R. Emparan, T. Harmark, V. Niarchos, N. A. Obers and M. J. Rodriguez, JHEP **0710** (2007) 110 [arXiv:0708.2181 [hep-th]].
- [10] B. Carter, Phys. Lett. B **228** (1989) 466;
B. Carter, Phys. Lett. B **238** (1990) 166 [hep-th/0703023 [hep-th]];
B. Carter, hep-th/9705172;
B. Carter, Int. J. Theor. Phys. **40** (2001) 2099 [gr-qc/0012036].
- [11] R. Emparan, T. Harmark, V. Niarchos and N. A. Obers, JHEP **1003** (2010) 063 [arXiv:0910.1601 [hep-th]].
- [12] B. Kleihaus, J. Kunz and E. Radu, Phys. Lett. B **718** (2013) 1073 [arXiv:1205.5437 [hep-th]].
- [13] Y. Lemperiere and E. P. S. Shellard, Phys. Rev. Lett. **91** (2003) 141601 [hep-ph/0305156].
- [14] E. Radu and M. S. Volkov, Phys. Rept. **468** (2008) 101 [arXiv:0804.1357 [hep-th]].
- [15] P. Grandclement, J. Comput. Phys. **229** (2010) 3334 [arXiv:0909.1228 [gr-qc]].
- [16] B. Kleihaus, J. Kunz and M. List, Phys. Rev. D **72** (2005) 064002 [arXiv:gr-qc/0505143];
B. Kleihaus, J. Kunz, M. List and I. Schaffer, Phys. Rev. D **77** (2008) 064025 [arXiv:0712.3742 [gr-qc]].
- [17] M. S. Volkov and E. Wöhnert, Phys. Rev. D **66** (2002) 085003.
- [18] R. A. Battye and P. M. Sutcliffe, Nucl. Phys. B **814** (2009) 180 [arXiv:0812.3239 [hep-th]].
- [19] D. J. Kaup, Phys. Rev. **172** (1968) 1331.

- [20] R. Ruffini and S. Bonazzola, Phys. Rev. **187** (1969) 1767.
- [21] M. S. Volkov and D. V. Gal'tsov, Phys. Rept. **319** (1999) 1 [hep-th/9810070].
- [22] R. Friedberg, T. D. Lee and A. Sirlin, Phys. Rev. D **13** (1976) 2739.
- [23] M. Colpi, S. L. Shapiro and I. Wasserman, Phys. Rev. Lett. **57** (1986) 2485.
- [24] R. M. Wald, *General Relativity*, University of Chicago Press, Chicago, (1984).
- [25] D. Kramer, H. Stephani, E. Herlt, and M. MacCallum, *Exact Solutions of Einstein's Field Equations*, Cambridge University Press, Cambridge, (1980).
- [26] J. L. Friedman, K. Schliech, and D. M. Witt, Phys.Rev.Lett. **71** (1993) 1486.
- [27] R. Bach and H. Weyl, Math. Zeit. **13** (1922) 132
- [28] S. Nishida and Y. Eriguchi, Ap. J. **427** (1994) 429.
- [29] F. E. Schunck and E. W. Mielke, Phys. Lett. A **249** (1998) 389.
- [30] B. Kleihaus and J. Kunz, Phys. Rev. Lett. **86** (2001) 3704.
- [31] B. Hartmann, B. Kleihaus, J. Kunz and M. List, Phys. Rev. D **82**, 084022 (2010) [arXiv:1008.3137 [gr-qc]].
- [32] O. J. C. Dias, G. T. Horowitz and J. E. Santos, JHEP **1107** (2011) 115 [arXiv:1105.4167 [hep-th]].
- [33] T. D. Lee and Y. Pang, Phys. Rept. **221** (1992) 251.
- [34] Y. Shnir, J. Phys. A **44** (2011) 425202 [arXiv:1101.5366 [hep-th]].
- [35] T. Wiseman, Class. Quant. Grav. **20** (2003) 1137 [arXiv:hep-th/0209051].
- [36] W. Schönauer and R. Weiß, J. Comput. Appl. Math. **27**, 279 (1989) 279;
M. Schauder, R. Weiß and W. Schönauer, *The CADSOL Program Package*, Universität Karlsruhe, Interner Bericht Nr. 46/92 (1992).
- [37] B. Kleihaus, J. Kunz, E. Radu and D. Senkbeil, Phys. Rev. D **83** (2011) 104050 [arXiv:1103.4758 [gr-qc]].
- [38] Y. Lemperiere and E. P. S. Shellard, Nucl. Phys. B **649** (2003) 511 [hep-ph/0207199].
- [39] B. Hartmann and B. Carter, Phys. Rev. D **77** (2008) 103516 [arXiv:0803.0266 [hep-th]].
- [40] S. Yoshida and Y. Eriguchi, Phys. Rev. D **56** (1997) 2.
- [41] R. Emparan and H. S. Reall, Class. Quant. Grav. **23** (2006) R169 [hep-th/0608012].
- [42] R. A. Battye and P. M. Sutcliffe, Nucl. Phys. B **805** (2008) 287 [arXiv:0806.2212 [hep-th]];
R. A. Battye, J. A. Pearson, S. Pike and P. M. Sutcliffe, JCAP **0909** (2009) 039 [arXiv:0908.1865 [hep-th]];
R. A. Battye and P. M. Sutcliffe, Phys. Rev. D **80** (2009) 085024 [arXiv:0908.1344 [hep-th]].
- [43] D. Mihalache, D. Mazilu, L.C. Crasovan, I. Towers, A.V. Buryak, B.A. Malomed, L. Torner, J.P. Torres, and F. Lederer, Phys. Rev. Lett. **88** (2002) 073902;
D. Mihalache, D. Mazilu, L.C. Crasovan, I. Towers, B.A. Malomed, A.V. Buryak, L. Torner, and F. Lederer, Phys. Rev. E **66** (2002) 016613;
D. Mihalache, D. Mazilu, I. Towers, B.A. Malomed, and F. Lederer, Phys. Rev. E **67** (2003) 056608.
- [44] J. Kunz, U. Neemann and Y. Shnir, Phys. Lett. B **640** (2006) 57 [hep-th/0606176].
- [45] J. Kunz, U. Neemann and Y. Shnir, Phys. Rev. D **75** (2007) 125008 [hep-th/0703232 [HEP-TH]].
- [46] H. Elvang and P. Figueras, JHEP **0705** (2007) 050 [hep-th/0701035].
- [47] H. Iguchi and T. Mishima, Phys. Rev. D **75** (2007) 064018 [arXiv:hep-th/0701043].
- [48] I. Pena and D. Sudarsky, Class. Quant. Grav. **14** (1997) 3131.
- [49] V. Cardoso, P. Pani, M. Cadoni and M. Cavaglia, Phys. Rev. D **77** (2008) 124044 [arXiv:0709.0532 [gr-qc]].
- [50] M. Ortaggio, JHEP **0505** (2005) 048 [arXiv:gr-qc/0410048].
- [51] P. Peter, Phys. Lett. B **298** (1993) 60.
- [52] B. Kleihaus, J. Kunz and Y. Shnir, Phys. Rev. D **68** (2003) 101701 [hep-th/0307215].
- [53] B. Kleihaus, J. Kunz and M. Leissner, Phys. Lett. B **663** (2008) 438 [arXiv:0802.3275 [hep-th]].
- [54] F. Navarro-Lerida and D. H. Tchrakian, Phys. Rev. D **81** (2010) 127702 [arXiv:0909.4220 [hep-th]].
- [55] M. S. Volkov, Phys. Lett. B **644** (2007) 203 [hep-th/0609112].
- [56] E. Radu and M. S. Volkov, Phys. Rev. D **79** (2009) 065021 [arXiv:0810.0908 [hep-th]].
- [57] B. Kleihaus, J. Kunz and M. Leissner, Phys. Lett. B **678** (2009) 313 [arXiv:0810.1142 [hep-ph]].